Resource

Cell Chemical Biology

In vivo bioluminescence imaging of granzyme B activity in tumor response to cancer immunotherapy

Graphical abstract

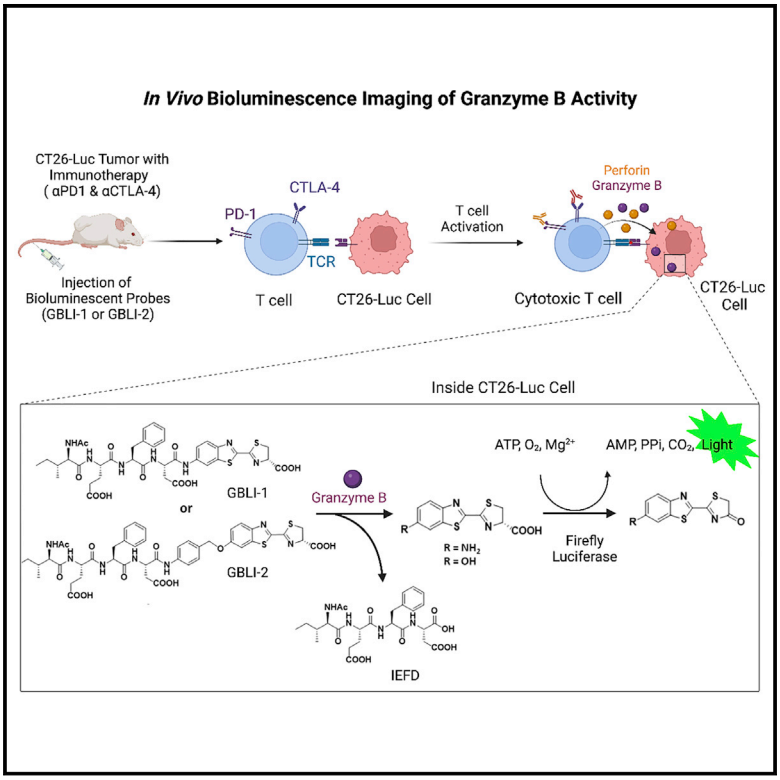

Authors

Min Chen, Kaixiang Zhou, Sheng-Yao Dai, ..., Liyang Cui, Juliana Idoyaga, Jianghong Rao

Correspondence

jrao@stanford.edu

In brief

Chen et al. report the first granzyme B-activated bioluminescent probe GBLI-2 for non-invasive, real-time, and longitudinal imaging *in vivo*. GBLI-2 imaging predicts therapeutic efficacy and correlates with the change in the population of PD-1 and granzyme B expressing $CD8^+$ T cells in tumors.

Highlights

- GBLI-2 is a bioluminescent probe that can be activated by granzyme B
- GBLI-2 bioluminescence emission increases by 284-fold upon granzyme B activation
- GBLI-2 can image granzyme B activity in tumors receiving PD-1/CTLA-4 antibodies
- GBLI-2 imaging can distinguish the responding tumors from non-responding tumors

Chen et al., 2022, Cell Chemical Biology *29*, 1556–1567
October 20, 2022
https://doi.org/10.1016/j.chembiol.2022.08.006

CellPress

Cell Chemical Biology

Resource

In vivo bioluminescence imaging of granzyme B activity in tumor response to cancer immunotherapy

Min Chen,[1,4] Kaixiang Zhou,[1,4] Sheng-Yao Dai,[1,4] Sirimuvva Tadepalli,[2] Preethi Bala Balakrishnan,[1] Jinghang Xie,[1] Fadi E.I. Rami,[2] Tingting Dai,[3] Liyang Cui,[1] Juliana Idoyaga,[2] and Jianghong Rao[1,3,5,*]

[1]Department of Radiology, Molecular Imaging Program at Stanford, Stanford University School of Medicine, Stanford, CA 94305, USA

[2]Department of Microbiology and Immunology, Stanford University School of Medicine, Stanford, CA 94305, USA

[3]Department of Chemistry, Stanford University, Stanford, CA 94305, USA

[4]These authors contributed equally

[5]Lead contact

*Correspondence: jrao@stanford.edu

https://doi.org/10.1016/j.chembiol.2022.08.006

SUMMARY

Cancer immunotherapy has revolutionized the treatment of cancer, but only a small subset of patients benefits from this new treatment regime. Imaging tools are useful for early detection of tumor response to immunotherapy and probing the dynamic and complex immune system. Here, we report a bioluminescence probe (GBLI-2) for non-invasive, real-time, longitudinal imaging of granzyme B activity in tumors receiving immune checkpoint inhibitors. GBLI-2 is made of the mouse granzyme B tetrapeptide IEFD substrate conjugated to D-luciferin through a self-immolative group. GBLI-2 was evaluated for imaging the dynamics of the granzyme B activity and predicting therapeutic efficacy in a syngeneic mouse model of CT26 murine colorectal carcinoma. The GBLI-2 signal correlated with the change in the population of PD-1- and granzyme B-expressing $CD8^+$ T cells in tumors.

INTRODUCTION

Immune checkpoint inhibitors (ICIs) work by blocking the co-inhibitory pathways of T cell activation (CTLA-4 and PD-1/PD-L1) and unleashing T cell cytotoxic function to kill tumor cells, which has produced stupendous clinical outcomes in a variety of cancer types (Bagchi et al., 2021; Del Paggio, 2018; Twomey and Zhang, 2021). Nonetheless, the success rate of ICI immunotherapy is still low in solid cancers and the ability to probe early immune response is instrumental in improving efficacy against poorly immunogenic tumors and preventing immune-related adverse events (de Miguel and Calvo, 2020; Hegde et al., 2016). In particular, ICI treatment is known to cause "pseudoprogression"—the apparent tumor size increase due to immune cell infiltration, which misleads tumor size measurement (Park et al., 2020). Biopsy offers a glimpse into predictive biomarkers but is limited by small sampling size and challenging to be performed repetitively due to its invasive nature (Topalian et al., 2016). Non-invasive imaging, in contrast, allows dynamic longitudinal monitoring of the whole tumor mass *in vivo* and is ideal for investigating the complex tumor immune microenvironment (Nishino et al., 2017; Patel et al., 2010; Saida et al., 2021). Positron emission tomography (PET) imaging has been developed to quantify the expression of checkpoint proteins and immune cell surface markers in tumors by using radiolabeled monoclonal antibodies against checkpoint proteins or T cell receptors and generated valuable insight. Although immunoPET holds high promise for clinical translation, it does not measure the immune cell functions, while T cell dysfunctions have been recognized as one of the major hurdles in the immune suppressive niche (Ng et al., 2022; Philip and Schietinger, 2022). Therefore, the activity-based imaging of T cell cytotoxicity in tumors has been proposed to serve as an early and direct indication of tumor response to ICI therapy. In this work, we explore bioluminescence imaging of the cytotoxic activity of tumor-infiltrating cytotoxic T lymphocytes (CTLs) in preclinical models.

Mechanistically, CTLs engage target cells through antigen binding and form immunological synapses, followed by degranulation of death-inducing effector molecules to exert cytotoxicity (Golstein and Griffiths, 2018; Weigelin et al., 2021). Among them, the serine protease granzyme B has been recognized as the primary effector enzyme in inducing target cell apoptosis (Cullen et al., 2010; Rousalova and Krepela, 2010). Based on its proteolytic property, fluorescent peptide substrate and genetic fusion with fluorescent proteins have long been used for imaging the granzyme B activity *in vitro* or in live cells (Bird et al., 2010; Choi and Mitchison, 2013; Packard et al., 2007). Until recently, imaging of granzyme B activity in whole living mice has been successfully demonstrated. Larimer et al. (2017) reported an inhibitor-based probe for PET imaging of granzyme B in a

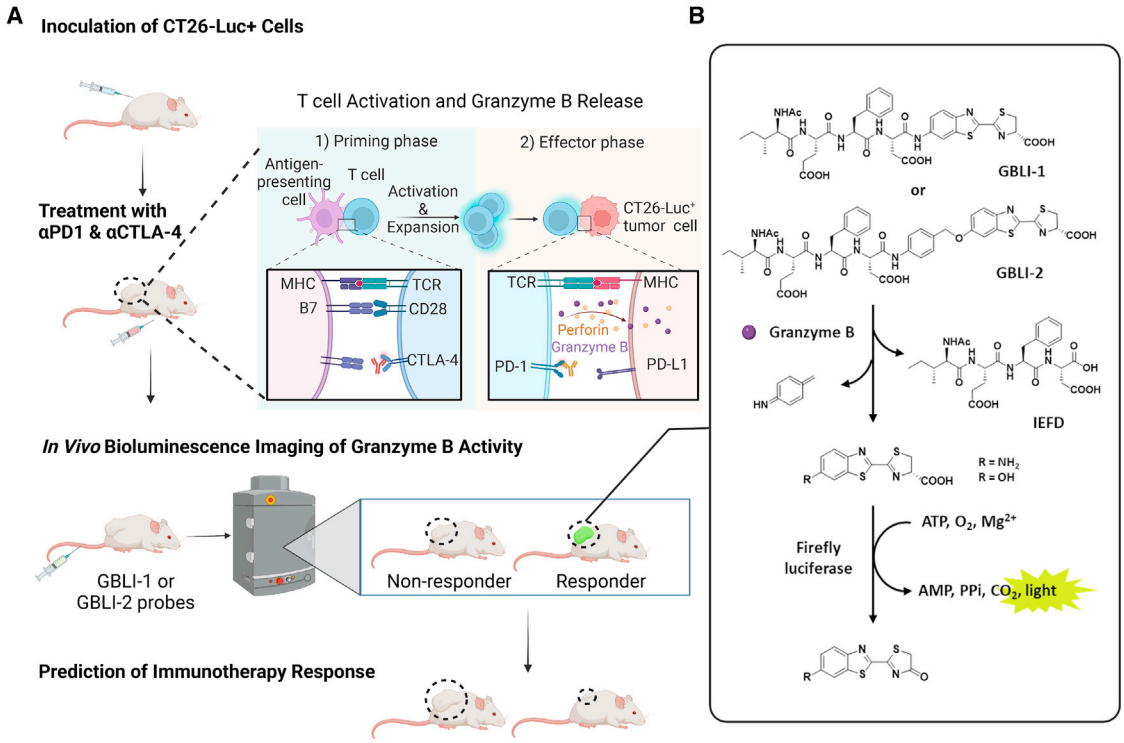

Scheme 1. Schematic illustration of the mechanism of bioluminescence imaging of granzyme B activity *in vivo* using GBLI probes

(A) BALB/c mice bearing CT26-Luc+ tumors are treated with checkpoint inhibitors (anti-PD-1 and anti-CLTA-4 antibodies) to block the inhibitory signaling toward cytotoxic T lymphocytes during both (1) priming and (2) effector phases to induce systemic immune response and release granzyme B to kill cancer cells. Mice are imaged with the bioluminescence imager by injecting GBLI probes to predict response before the divergence of tumor volume is evident.

(B) In responders, the discharged granzyme B from CTLs cleaves GBLI probes to generate free luciferins, which will be processed by firefly luciferase in CT26-Luc+ cells to emit bioluminescence. Part of this scheme was created with BioRender.com.

syngeneic murine model of colon adenocarcinoma. Near-infrared fluorescence, photoacoustic, and chemiluminescence activatable probes have also been developed to conduct *in vivo* detection of granzyme B activity in several animal models from cancer immunotherapy to organ transplantation (He et al., 2020; Mac et al., 2019; Scott et al., 2021; Xie et al., 2022; Zhang et al., 2021; Zhao et al., 2021).

Bioluminescent emission occurs during the catalytic reaction between the luciferase enzyme and its substrate luciferin, thus providing high sensitivity (without autofluorescence) and high specificity (confined to luciferase-expressing cells), as well as permitting repetitive imaging due to rapid body clearance (Zambito et al., 2021). Although the requirement of introducing the luciferase-gene generally limits bioluminescence imaging in patients, it has been widely used in chemical biology for monitoring tumor growth, cell trafficking, and protein-protein interactions in preclinical models (Love and Prescher, 2020; Syed and Anderson, 2021; Yeh and Ai, 2019). Caged luciferin substrates are developed and employed to detect the activity of enzymes overexpressed by cancer cells (Su et al., 2019). To harness the power of bioluminescence imaging for real-time monitoring of immune response, we aimed at developing an activatable probe targeting granzyme B secreted by tumor infiltrating CTLs to directly monitor tumor responding *in vivo* (Scheme 1A). To demonstrate the use of these probes, we developed a syngeneic murine colorectal carcinoma model with CT26 cells transgenic expression firefly luciferase receiving ICI treatments. Using this platform, we showed that one of the designed probes, GBLI-2, produced bioluminescence signals specifically upon granzyme B cleavage and reported the activity of granzyme B in response to the immunotherapy. Tumors responding to ICI treatment have displayed significantly higher bioluminescent signals than the non-responding and untreated tumors, which was consistent with the increased level of PD-1- and granzyme B-expressing $CD8^+$ CTLs. We further applied the probe in a tumor-rechallenging model to successfully image the granzyme B activity generated from a long-lasting immunological memory. We believe the development of this bioluminescence probe can facilitate the monitoring of immune response in animal models and accelerate the advancement of immunotherapy.

RESULTS

Design and biochemical characterization of granzyme B bioluminescence probes

Granzyme B is the primary mediator enzyme of CTL cytotoxicity and accomplishes this effect through proteolytic cleavage of Bid and activation of caspases to induce apoptosis in target cells. Previous screening of peptide combinatorial libraries has identified the differential optimal tetrapeptides (P4–P1) for human and mouse granzyme B (Casciola-Rosen et al., 2007): Ile-Glu-Pro-Asp (IEPD) for human and Ile-Glu-Phe-Asp (IEFD) for mouse.

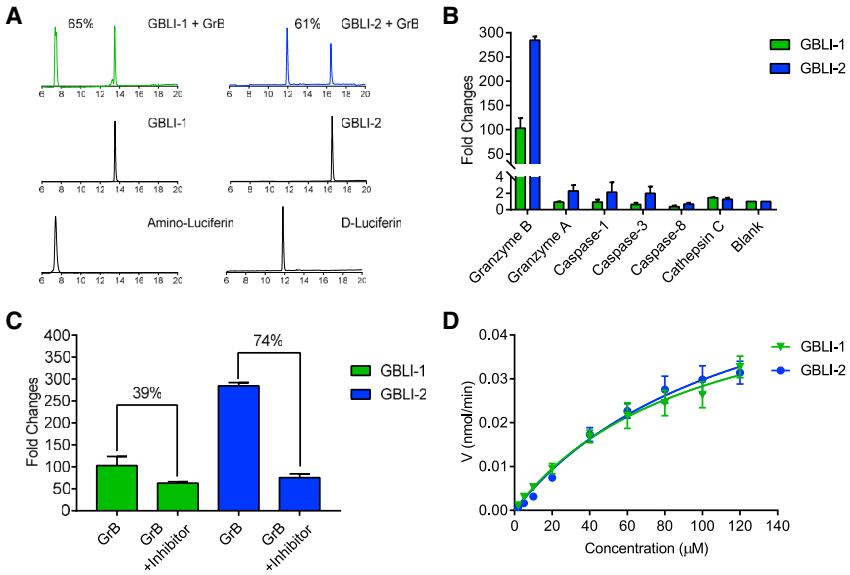

Figure 1. *In vitro* characterization of GBLI-1 and GBLI-2 in response to granzyme B

(A) HPLC traces of GBLI-1 and GBLI-2 (10 μM) in the absence or presence of mouse granzyme B (22 nM, 24 h).

(B) Enzyme-specific activation of GBLI-1 and GBLI-2 probes. Two GBLI probes were incubated with different enzymes in the corresponding buffer at 37°C for 24 h.

(C) Effects of granzyme B (GrB) inhibitors (100 μM) on GBLI-1 and GBLI-2 in 50 mM Tris buffer with 100 μg/mL luciferase, 10 mM $MgCl_2$, and 1 mM ATP.

(D) Nonlinear regression analysis of granzyme B cleavage rate V (nmol/min) of GBLI-1 and GBLI-2 probes. Various concentrations of GBLI-1 and GBLI-2 (2, 5, 10, 20, 40, 60, 80, 100, and 120 μM) probes were incubated with mouse granzyme B (22 nM) in Tris buffer (50 mM [pH 7.4]) at 37°C and monitored in real time for 30 min using a microplate reader. Error bars represent ±SD, n = 3 replicates.

Our study focused on mouse models that led to the choice of IEFD in designing granzyme B bioluminescence (GBLI) probes. Caging of luciferin analogs at the 4′ and 6′ positions is known to prohibit the firefly luciferase recognition and reactivity to catalyze the light-emitting reaction until the triggering of cleavage (Miska and Geiger, 1987; Su et al., 2019). Direct conjugation of peptide substrates to 6′-amino-D-luciferin has been applied to develop the bioluminescent probes for imaging the proteases, such as caspase-3/7 (O'Brien et al., 2005) and furin (Dragulescu-Andrasi et al., 2009). We first designed GBLI-1 by using this approach with the IEFD peptide. To compare the effect of using D-luciferin (with a 6′-hydroxy group), we introduced a self-immolative linker (Yao et al., 2007) to connect the IEFD tetrapeptide in constructing GBLI-2 (Scheme 1B). GBLI-1 and GBLI-2 probes were synthesized (Scheme S1) and characterized by nuclear magnetic resonance (^{1}H-NMR and ^{13}C-NMR) and high-resolution mass spectrometry (Figures S1 and S2).

We first tested whether the probes could be cleaved by recombinant mouse granzyme B. GBLI-1 and GBLI-2 were incubated with granzyme B (22 nM) in Tris buffer (50 mM [pH 7.5]) for various times (0.5, 3, 6, 12, and 24 h), and the reaction mixtures were analyzed by high-performance liquid chromatography (HPLC) (Figures 1A and S3). New peaks corresponding to amino-D-luciferin (T_R = 8 min) and D-luciferin (T_R = 12 min) were detected on HPLC, confirming the expected cleavage by granzyme B. GBL1-1 showed 65% cleavage after 24 h incubation, whereas 61% cleavage of GBLI-2 was observed. To investigate the selectivity of GBLI-1 and GBLI-2 toward granzyme B, we incubated them with granzyme A, granzyme B, caspase-1, caspase-3, caspase-8, cathepsin C, or PBS buffer as a blank group, respectively (Figure 1B). It was found that, upon granzyme B incubation, after the addition of luciferase, ATP, and $MgCl_2$, GBLI-1 and GBLI-2 exhibited a 103- and 284-fold increase in bioluminescence signals, respectively. In contrast, their incubation with active caspases (caspase-1, caspase-3, and caspase-8), granzyme A, and cathepsin C produced bioluminescence signals similar to that of the PBS blank. The cleavage of GBLI probes by granzyme B could be blocked by inhibitor Ac-IEPD-CHO, resulting in decreased bioluminescence signal by 39% for GBLI-1 and 74% for GBLI-2 (Figure 1C). The enzymatic Michaelis-Menten constants (K_m) of hydrolysis of GBLI-1 and GBLI-2 by granzyme B were calculated to be 97.4 and 123.2 μM, respectively (Figure 1D). The catalytic rate constants (k_{cat}) of GBLI-1 and GBLI-2 were 0.067 and 0.080 s^{-1}, respectively. The catalytic efficiencies (k_{cat}/K_m) of GBLI-1 and GBLI-2 by granzyme B were 687.9 and 649.4 L $mol^{-1}s^{-1}$, respectively. These values are comparable with those reported for the tetrapeptide substrates (Casciola-Rosen et al., 2007). The difference in emission despite similar cleavage yields of GBLI probes can be explained by the fact that amino-D-luciferin has a higher affinity to luciferase, and thus has a more pronounced product inhibition resulting in less photon flux (Reddy et al., 2010). Overall, both GBLI-1 and GBLI-2 can be specifically uncaged by granzyme B, while GBLI-2 showed better sensitivity than GBLI-1.

In vitro bioluminescence imaging of granzyme B

The ability of GBLI-1 and GBLI-2 to detect granzyme B activity was first measured in Tris buffer (50 mM [pH 7.4]). Both probes gave bright bioluminescence that gradually decayed over time (approximately 90 min) (Figures 2A and 2B). The initial signal from GBLI-2 was 2.5-fold stronger than that of GBLI-1. We then pursued to evaluate the GBLI probes in cell lysates of CT26 murine colon cancer cells transfected with the luciferase gene (CT26-luc). GBLI probes were preincubated with granzyme B in Tris buffer (50 mM [pH 7.4]) overnight, and were mixed with CT26-luc lysates to measure the bioluminescence signal (Figures 2C and 2D). For GBLI-1, the bioluminescence signal (7.4 ± 1.1 × 10^5 p/s/cm^2/sr) was approximately two times that of the control CT26-luc lysates where GBLI-1 was not preincubated with granzyme B (3.6 ± 1.6 × 10^5 p/s/cm^2/sr). In contrast, GBLI-2 emitted 6.6-fold higher signals (1.6 ± 0.1 × 10^6 p/s/cm^2/sr) than that without granzyme B preincubation (2.1 ± 0.3 × 10^5

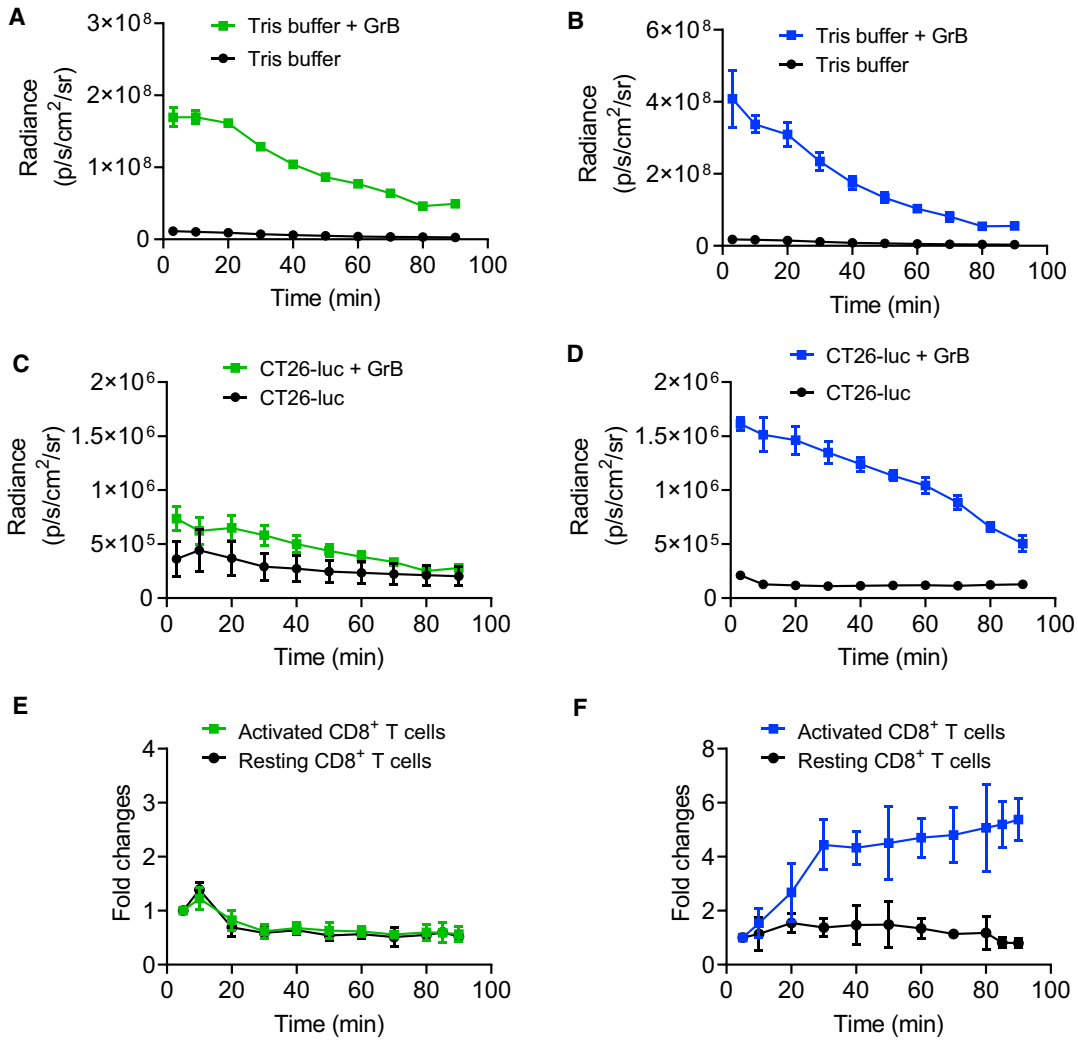

Figure 2. Detection of bioluminescence signals in activation of granzyme B using GBLI-1 and GBLI-2 probes

Dynamic bioluminescence changes of GBLI-1 (A, C, and E) or GBLI-2 (B, D, and F) probes in Tris buffer. GBLI probes were preincubated with granzyme B in Tris-buffer (50 mM [pH 7.4]) for 24 h and then incubated with Tris buffer (50 mM [pH 7.4]) containing 100 μg/mL luciferase, 1 mM ATP, and 10 mM $MgCl_2$ over 90 min. (C and D) Dynamic BL changes of GBLI-1 or GBLI-2 probes in CT26-luc cell lysates. GBLI probes were preincubated with granzyme B enzyme overnight and then incubated with CT26-luc cell lysates over 90 min. (E and F) The fold changes of bioluminescence signals of GBLI-1 or GBLI-2 probes in $CD8^+$ T cell lysates. GBLI probes were incubated with activated $CD8^+$ T cell lysate or resting $CD8^+$ T cells lysates over 90 min. Error bars represent ±SD, n = 3 replicates.

p/s/cm^2/sr). After 90 min incubation, the bioluminescence signals from the GBLI-1 probe showed no statistically significant difference between CT26-luc cell lysates with ($2.0 \pm 0.9 \times 10^5$ p/s/cm^2/sr) or without ($2.8 \pm 1.4 \times 10^5$ p/s/cm^2/sr) granzyme B preincubation (Figure 2C) but, for GBLI-2, the signal from granzyme B preincubated samples remained higher ($5.1 \pm 0.8 \times 10^5$ p/s/cm^2/sr) than cell lysates without granzyme B ($1.3 \pm 0.1 \times 10^5$ p/s/cm^2/sr) (Figure 2D). These results indicated that GBLI-2 was more sensitive to granzyme B detection and had a lower non-specific background in CT26-luc cell lysates than GBLI-1.

We also tested the GBLI probes for detecting granzyme B innately expressed by activated cytotoxic $CD8^+$ T cells (Figures 2E and 2F). The $CD8^+$ T cells were isolated from the spleen of transgenic BALB/c mice with luc+ lymphocytes, and their purity was confirmed by flow cytometry (Figures S4A–S4C). The isolated $CD8^+$ T cells were either used without further manipulation (as resting $CD8^+$ T cells) or activated *ex vivo* using the protocol described in the STAR Methods (as activated $CD8^+$ T cells). The expression of granzyme B was low in resting $CD8^+$ T cells and high in activated $CD8^+$ T cells, as shown by western blotting (Figure S4D). Incubation of GBLI-1 with activated $CD8^+$ T cell lysate showed a poor bioluminescence signal, nearly similar to that in resting $CD8^+$ T cells (Figure 2E), whereas incubation of GBLI-2 with activated $CD8^+$ T cell lysates resulted in a 4.4-fold increase in bioluminescence signal over resting $CD8^+$ T cells (Figure 2F). When we tested both probes in live $CD8^+$ T cells, no statistically significant different bioluminescent

signals were observed between resting and activated $CD8^+$ T cells (Figures S4E and S4F). This observation may reflect poor cell permeability of GBLI-2 and also low granzyme B activity in granules due to acidic pH and serpin proteinase inhibitors (Trapani, 2001). Collectively, these results showed that GBLI-2 was more sensitive and specific than GBLI-1 in the detection of the released granzyme B activity. Therefore, we applied GBLI-2 to real-time imaging of granzyme B activity *in vivo*.

In vivo bioluminescence imaging of granzyme B in immunotherapy

BALB/c mice bearing CT26-luc tumors were treated with combination immunotherapy (co-administration of PD-1 and CTLA-4 checkpoint inhibitors) on days 12, 15, and 18 after tumor implantation (Figure 3A). Bioluminescence images were longitudinally acquired and quantified after intravenous injection with GBLI-2 (Figures 3B–3E and S5A). The bioluminescence signals in treatment-responsive tumors gradually increased and reached the maximum on day 17 post tumor implantation with an intensity of $1.6 \pm 0.3 \times 10^5$ p/s/cm^2/sr, which was 3.5-fold higher than that in non-responding ($0.4 \pm 0.1 \times 10^5$ p/s/cm^2/sr) and untreated mice ($0.3 \pm 0.03 \times 10^5$ p/s/cm^2/sr). In comparison, the bioluminescence signals of GBLI-2 in both non-responding and untreated tumors were much lower and increased slightly over time, which likely resulted from more firefly luciferase reporter expression in growing tumors. To monitor the level of firefly luciferase due to the CT26-luc tumor growth, mice were injected with D-luciferin at 2 h after GBLI-2 imaging (Figure 3D). The bioluminescence signals from D-luciferin in responding mice gradually decreased due to tumor regression. In contrast, the signals of D-luciferin in non-responding and untreated tumors increased over time due to tumor growth.

To correct the effect of varying levels of firefly luciferase among tumors on the activity of granzyme B released by cytotoxic $CD8^+$ T cells, we normalized the GBLI-2 signal by dividing its value by the D-luciferin signal (Figure 3E). On day 11 after tumor inoculation (before immunotherapy), the ratio of GBLI-2/D-luciferin was comparable among three groups: $2.9 \pm 0.3 \times 10^{-4}$ for responding tumors, $3.2 \pm 0.6 \times 10^{-4}$ for non-responding tumors, and $4.3 \pm 0.1 \times 10^{-4}$ for untreated tumors ($p > 0.05$). We also measured the ratio of GBLI-2 and D-luciferin signals in NSG and nude mice to check non-specific background (Figure S5B), and the result showed that there was no significant difference in the ratio of GBLI-2/D-luc between the immunocompetent BALB/c, T cell-deficient nude, and immunodeficient NSG mice. After immunotherapy, the ratio in responding tumors increased to $1.7 \pm 0.3 \times 10^{-3}$ on day 17 and to $4.4 \pm 1.0 \times 10^{-3}$ on day 23. For non-responding tumors, the ratio decreased to $5.9 \pm 2.9 \times 10^{-5}$ on day 17 and to $1.8 \pm 0.7 \times 10^{-5}$ on day 23. A similar trend was observed for untreated tumors: $6.0 \pm 2.0 \times 10^{-5}$ on day 17 and $1.4 \pm 0.9 \times 10^{-5}$ on day 23. The GBLI-2/D-luciferin ratio changes during immunotherapy inversely correlated with the tumor volumes Figure 3F): the tumor volumes in non-responding and untreated mice increased over time, but their ratios decreased; in the responding tumors, the tumor started to shrink as the ratio increased. These results have established the ability of GBLI-2 for non-invasive imaging of granzyme B activity *in vivo* and monitoring tumor response to checkpoint inhibitors treatment.

In vivo bioluminescence imaging of granzyme B in a tumor rechallenge model

It has been reported that mice cured of CT26 tumors displayed long-term memory and were able to reject CT26 tumors upon rechallenge (Sagiv-Barfi et al., 2015). We were interested in imaging the granzyme B activity with the GBLI-2 probe in the tumor rechallenge model. The mice cured of their primary CT26-luc tumors after checkpoint inhibitors treatment were rechallenged with either CT26-luc colon or 4T1-luc breast cancer cells in the lower flank at 110 days after initial tumor implantation (Figure 4A). We observed that the GBLI-2 bioluminescent signal drastically increased in CT26-luc-rechallenged mice (Figure 4B) compared with the mice rechallenged with 4T1-luc tumors (Figure 4C). The signals reached a peak on day 2 after the CT26-luc rechallenge ($6.1 \pm 1.1 \times 10^4$ p/s/cm^2/sr) and then gradually decreased on day 4 ($4.2 \pm 2.1 \times 10^4$ p/s/cm^2/sr) and day 6 ($2.2 \pm 0.2 \times 10^4$ p/s/cm^2/sr). The increase in the GBLI-2 signal may be due to an increase in infiltration of memory $CD8^+$ T cells expressing granzyme B into the site of CT26-luc tumor injection upon antigen recognition. This CT26-luc rechallenge also showed a decrease in the D-luciferin signal, reflecting the inability of the injected CT26-luc cells to establish a tumor. Together, this resulted in a gradual, steady increase in the GBLI-2/D-luciferin ratio over time (Figure 4D), as observed in treatment-responding mice (Figure 3E). In contrast, there was only a slight change in the GBLI-2 signal in the 4T1 rechallenge model on days 2, 4, and 6 after rechallenging ($1.1 \pm 0.2 \times 10^4$, $2.3 \pm 0.8 \times 10^4$, and $2.0 \pm 1.0 \times 10^4$ p/s/cm^2/sr, respectively), corresponding to a progressive increase in tumor volume as measured by the D-luciferin bioluminescence signal. This result may be interpreted as the CT26 antigen-trained $CD8^+$ T cells failed to recognize 4T1 tumor cells. The ratio of GBLI-2/D-luciferin thus decreased in comparison with the CT26 rechallenge (Figure 4E). These results indicated that GBLI-2 could real-time monitor the granzyme B activity in the rechallenge model with anti-tumor immunity.

Ex vivo assessment of immunotherapy response

We next evaluated whether the bioluminescent signals of GBLI-2 *in vivo* correlated with the immune response by *ex vivo* analysis of the T cells in the tumor. Tumors at 17 days post tumor inoculation were collected for flow cytometry and immunofluorescence staining (Figure 5). Treated mice were grouped as responding and non-responding based on the GBLI-2 bioluminescence imaging. We found that responding treated mice harbored a significantly higher infiltration of $CD8^+$ T (42.4% ± 20.9% of $CD8^+$ T cells) compared with non-responding (11.5% ± 8.5% of $CD8^+$ T cells) and untreated (8.0% ± 7.3% of $CD8^+$ T cells) mice (Figure 5A) ($p < 0.01$). Furthermore, $CD8^+$ T cells from responding treated mice expressed higher levels of PD-1 (32.2% ± 13.4% of PD1+/CD8+ T cells) when compared with the non-responding (3.1% ± 4.9% of PD-1+/CD8+ T cells) and untreated (0.8% ± 1.2% of PD-1+/CD8+ T cells) mice ($p < 0.005$) (Figure 5B). We then questioned if the ability of $CD8^+$ T cells to secrete granzyme B correlated with the GBLI-2 bioluminescence imaging (Figure 5C). Indeed, treated responding mice harbored a significantly higher number of $CD8^+$ T cells producing granzyme B (23.2% ± 9.7% of granzyme B+/CD8+ T cells) when compared with non-responding

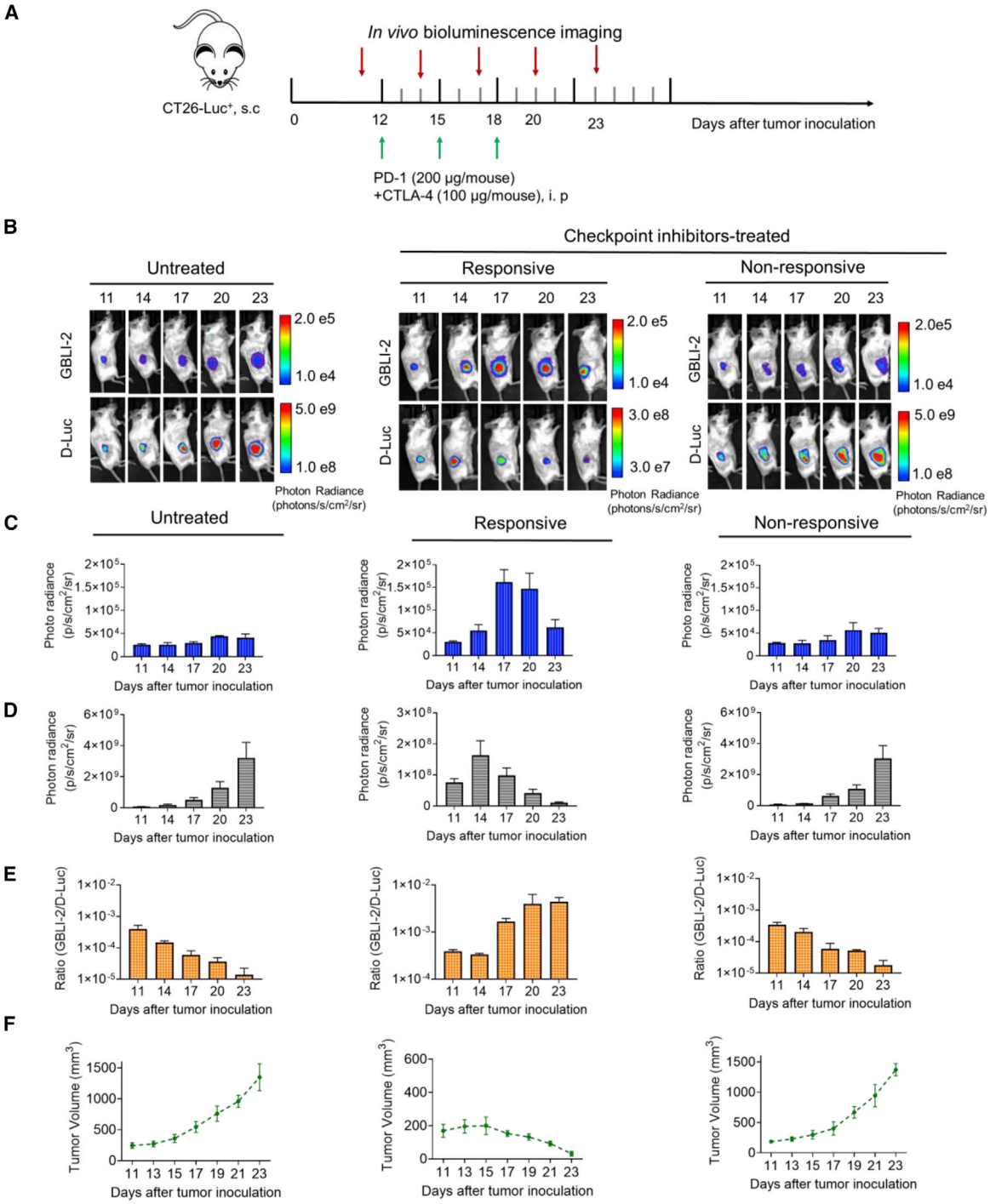

Figure 3. Real-time bioluminescence imaging of immunotherapy response in BALB/c mice bearing CT26-luc tumors using GBLI-2

(A) Scheme showing the experimental design to evaluate the immunotherapy response *in vivo*. Mice bearing CT26-luc tumors after immunotherapy were imaged with the Lago-X system.

(B) Representative bioluminescence images of granzyme B activity in mice injected with GBLI-2 probes (i.v., 10 mg/kg in 100 μL of saline) and then, after 2 h, mice were injected with D-luciferin (D-Luc) for monitoring tumor growth. Imaging was performed on days 11, 14, 17, and 20 after tumor inoculation.

(C and D) Quantification of GBLI-2 (C) and D-Luc (D) signals at different time points.

(E) The ratios of GBLI-2 and D-Luc signals.

(F) Tumor volume measurement of CT26-luc tumors in three groups over 23 days. Error bars represent ±SD, n = 5 animals per group.

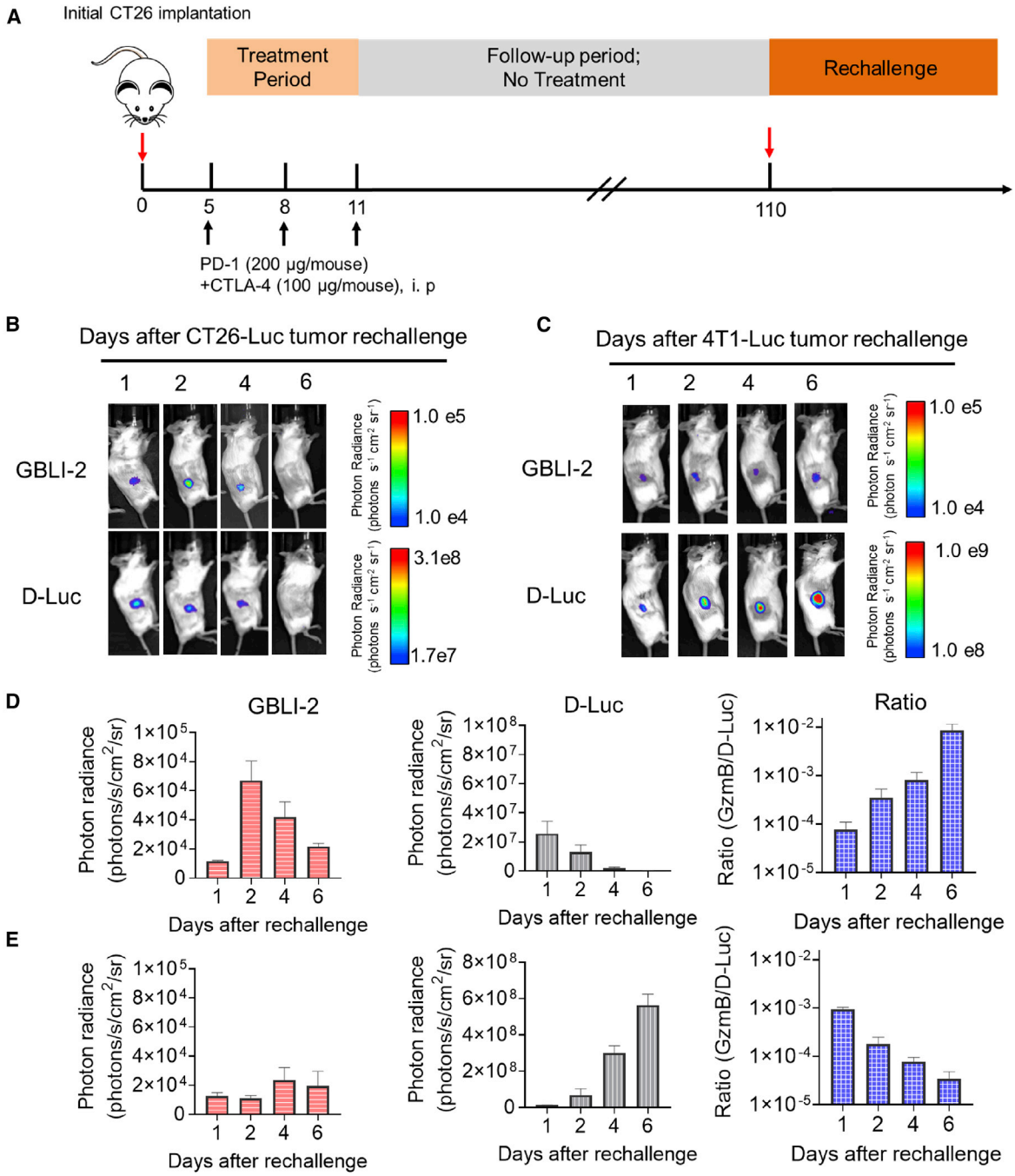

Figure 4. Real-time bioluminescence imaging of granzyme B activity in tumor rechallenge models using GBLI-2 probes

(A) Scheme showing the rechallenge experimental design to evaluate the immune memory effect *in vivo*.

(B–E) The dynamic BLI images of rechallenged mice with CT26-luc or 4T1-luc cells for 6 days.

(D and E) Quantification of the BLI signal intensity of rechallenge models with CT26-luc (D) or 4T1-luc cells (E). Error bars represent ±SD, n = 5 animals per group.

(2.9% ± 2.9% of granzyme B+/CD8 T cells) and untreated (1.1% ± 1.0% of granzyme B+/CD8+ T cells) mice ($p < 0.005$). $CD8^+$ T cells producing granzyme B in responding groups also expressed higher levels of PD-1 (Figure 5D). These results are in good agreement with the immunofluorescence staining and imaging (Figure 5E). In treated responding mice, there were high intensities of both granzyme B and CD8 staining, but a low intensity of granzyme B and CD8 in treated non-responding and untreated tumors. Taken together, we have shown that the population of PD-1- and granzyme B-expressing $CD8^+$ T cells was significantly elevated in CT26-luc tumor response to immunotherapy with checkpoint inhibitors treatment, which strongly correlates with the bioluminescence imaging result of the granzyme B activity by GBLI-2.

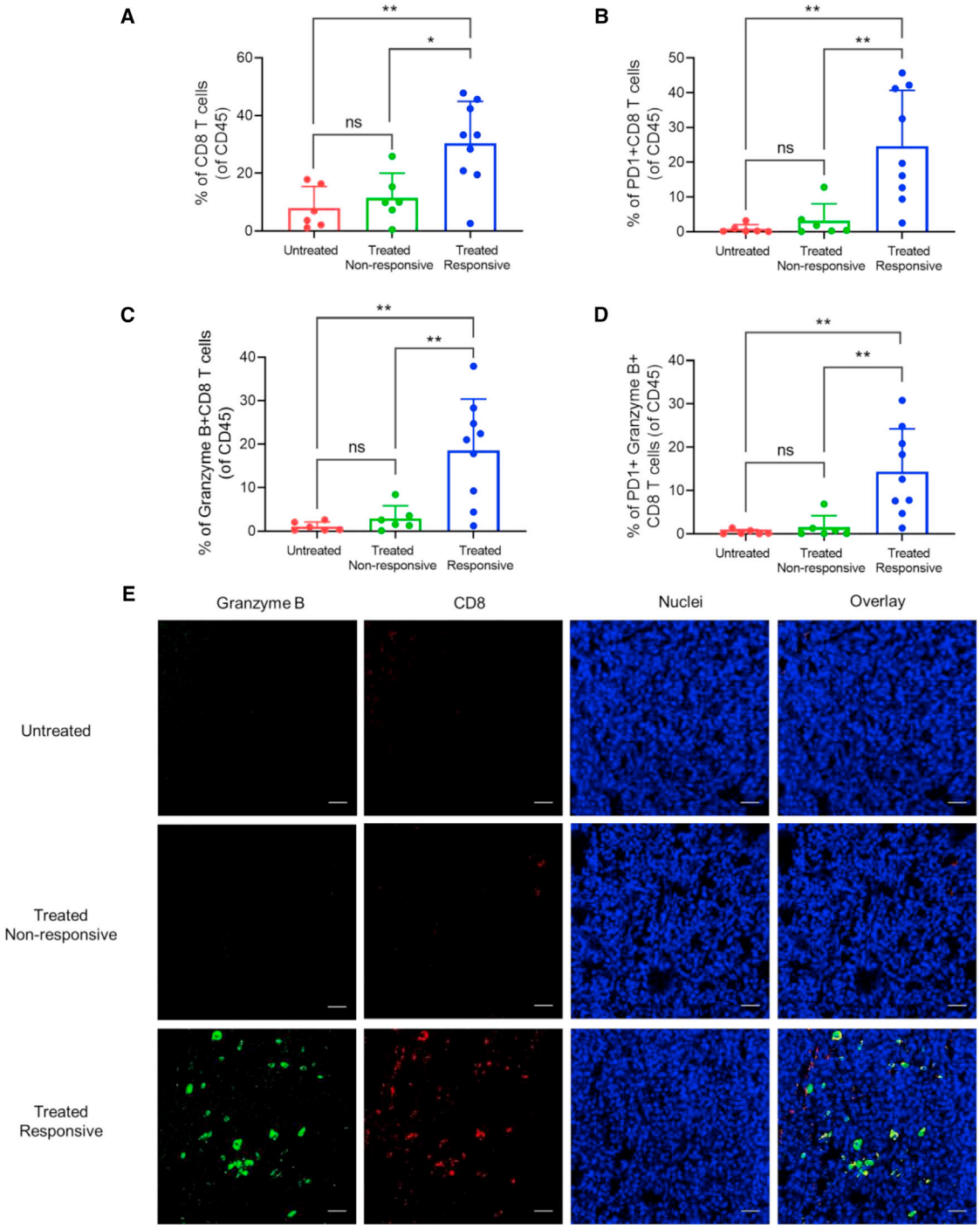

Figure 5. *Ex vivo* analysis of tumors after checkpoint inhibitor treatment

(A–D) On day 17 after tumor inoculation, tumors from untreated, treated non-responsive, or treated responsive groups were analyzed using flow cytometry. (A) Frequency of $CD8^+$ T cells in CT26 tumors. (B) Frequency of $PD1^+$ $CD8^+$ T cells. (C) Frequency of granzyme B^+ $CD8^+$ T cells. (D) Frequency of granzyme B^+ PD-1^+ $CD8^+$ T cells. All cells were gated on $CD45^+$ lymphocytes, n = 6–8 tumor samples per group.

(E) Representative immunofluorescence staining of granzyme B (green), CD8 (red), and nuclei (DAPI, blue) to show differential staining in responder, non-responder, and untreated tumors. Scale bar, 40 μm. Statistics were done using one-way ANOVA. *$p < 0.05$, **$p < 0.01$. Error bars represent ±SD.

DISCUSSION

Cancer immunotherapy harnesses the power of the patient's own immune system to attack and kill tumor cells and has revolutionized cancer treatment. The dynamic nature of the immune response and the low efficacy of current ICI immunotherapy, however, pose the need for the development of non-invasive imaging techniques to monitor immune cell functions in living subjects. Granzyme B, a key member of the granule enzyme (or granzyme) family expressed by CTLs and nature killer (NK) cells, has recently emerged as an imaging marker of the cytotoxic activity of immune cells. In this work, we designed bioluminescent probes for imaging the activity of granzyme B in mice receiving immune checkpoint blockade therapy. GBLI-1 follows the common design of protease-activated bioluminescent probes in coupling the peptide substrate of granzyme B with the substrate of firefly luciferase, amino-D-luciferin. GBLI-2, on the other hand, contains a self-immolative linker to enable the caging of D-luciferin that generates brighter bioluminescence emission than amino-D-luciferin (Liu et al., 2018). Therefore, GBLI-2 displayed better sensitivity in imaging the granzyme B activity. The linker design in GBLI-2 may also be applied to other proteases and can afford a similar improvement in sensitivity. The sensitivity and selectivity of GBLI-2 may be further improved with the use of optimal unnatural amino acid-based granzyme B substrate sequences (Janiszewski et al., 2020).

It is reported that the transcription and expression of granzyme B in T lymphocytes are regulated and induced only following exposure to a specific antigen or stimulations (Trapani, 2001). This was confirmed in our western blot analysis (Figure S4D), in which isolated $CD8^+$ T cells co-stimulated (active) by anti-CD3/CD28 showed a significantly higher amount of granzyme B than that of unstimulated (resting). The activity of intracellular stored granzyme B in cytotoxic granules is inhibited by acidic pH and serpin inhibitors. A few studies report that granzyme B retains partial activity in granules (Janiszewski et al., 2020; Xie et al., 2022). When we applied our GBLI probes to image the endogenously expressed granzyme B, we found no increase in signal when the probes were incubated with live isolated luc+ $CD8^+$ T cells even with the co-stimulations (Figure S4F). This result may also reflect the poor cell permeability of GBLI probes. Therefore, the bioluminescence signals observed in tumor milieu *in vivo* likely came from the cleavage of GBLI-2 by extracellular granzyme B discharged from activated tumor-infiltrating CTLs.

Using a CT26 colon cancer mouse model, we showed that the GBLI-2 probe was able to repetitively image the activity of granzyme B for monitoring tumor response to ICI treatments (Figure 3). GBLI-2 signals showed a significant increase in treatment-responding tumors 5 days after the first ICI injection, while there was just a small increase in non-responding and untreated tumors due to the increase of luciferase activity from tumor growth (Figure 3C). The increase in the granzyme B activity correlated well with a larger population of $CD8^+$ T cells expressing granzyme B and PD-1 in responding tumors determined from flow cytometry. The $CD8^+$ T cell population in non-responded tumors showed no statistically significant difference from that in untreated tumors (Figure 5A). The variation in the $CD8^+$ T cell population among treated CT26 tumors underscores the importance of developing an imaging biomarker to evaluate the immune response. Consistent with other studies (Larimer et al., 2017; Nguyen et al., 2020), tumors with high GBLI-2 signals shrank in size and regressed, and those with low GBLI-2 signals progressed similar to untreated control, confirming the value of granzyme B imaging for predicting the therapeutic outcome. We also applied GBLI-2 to image the activity of granzyme B in the tumor-rechallenging model (Figure 4). During the rechallenge, mice previously responding to ICI treatment rapidly eliminated CT26 but not 4T1 tumor cells, suggesting that long-lasting immunological memory was established in these mice. Correspondingly, GBLI-2 bioluminescence imaging revealed rapidly increased granzyme B activity on day 2 after the rechallenge (Figure 4D).

Compared with other granzyme B imaging strategies, GBLI-2 bioluminescence imaging displays several advantages in monitoring response to immunotherapy in the preclinical models. Unlike PET, bioluminescence imaging is more widely accessible, is of low cost, and does not use radioactivity. GBLI-2 imaging of the granzyme B activity shows excellent signal-to-noise ratios and high sensitivity. In comparison with fluorescent nanoparticles that are often cleared slowly from the body (Nguyen et al., 2020), GBLI-2 permits repetitive injections to capture the dynamics of the granzyme B activity in real time. We found that the granzyme B activity reached the peak 5 days after the initiation of the ICI treatment.

Limitations of the study

GBLI-2 imaging requires a genetic introduction of a bioluminescent reporter like firefly luciferase. When firefly luciferase is expressed in tumor cells, the activity of the firefly luciferase may change in response to treatment and thus can impact the GBLI-2 bioluminescence signal. This effect, however, can be corrected by subsequent bioluminescence imaging with D-luciferin. Applying it to normalize the GBLI-2 signal then affords the ratio of the GBLI-2 to D-luciferin signal that can report the activity of granzyme B independent of the level of firefly luciferase (Figure 3E). On the other hand, firefly luciferase may be introduced to immune cells. In such a case, bioluminescence imaging is applied in quantifying immune infiltration with transgenic mice or with adaptively transferred T cells expressing luciferase (Xie et al., 2022). Application of GBLI-2 to these models potentially can report the immune cell activity but may result in higher background signals generated by the basal activity of granzyme B in the immune cell populations. In addition, luciferase as a foreign gene may generate immunogenicity that compromises the growth and invasiveness of the reporter-expressing tumor cells (Baklaushev et al., 2017). For us, rejections of CT26-luc tumor implantation in BALB/c mice were observed to a less extent, but the use of reporter luciferase may present a limitation in some immunological experiments.

In conclusion, this work reports the development of the bioluminescent probe GBLI-2 for imaging the activity of granzyme B *in vivo*. The utility of the probe has been demonstrated in imaging immune response to ICI treatments in a syngeneic mouse model of CT26 murine colorectal carcinoma. The GBLI-2 signal has been found to correlate with the tumor burden change in predicting therapeutic efficacy and reflected the change in the population of PD-1- and granzyme B-expressing $CD8^+$ T cells in tumors.

In addition to cancer immunotherapy, granzyme B is also involved in inflammatory and autoimmune diseases (Boivin et al., 2009), such as autoimmune disease (Russo et al., 2018), skin disorders (Turner et al., 2019), and type 1 diabetes (Thomas et al., 2010). GBLI-2 may find applications in imaging granzyme B activity in these disease models too.

SIGNIFICANCE

Cancer immunotherapy, which harnesses the host immune system to combat malignant cells and immune checkpoint inhibitors (ICIs), has transformed the treatment regime against various cancers. However, the number of patients who have durable response to the ICI therapy is currently small. Many malignant tumors in cancer patients can employ complicated mechanisms to evade immune surveillance. Non-invasive imaging is a powerful tool to probe the complex tumor immune microenvironment through dynamic longitudinal monitoring of the whole tumor mass *in vivo*. As a primary preclinical imaging technique, bioluminescence imaging offers advantages, such as high sensitivity and high specificity for cancer imaging. To harness the power of bioluminescence imaging for real-time monitoring of immune response, in this study, we targeted granzyme B, the primary enzyme secreted by the cytotoxic effector T cells and developed a bioluminescent probe for non-invasive *in vivo* imaging of granzyme B activity. Of the two probes designed and characterized, GBLI-2 gave strong bioluminogenic responses selectively to granzyme B and allowed longitudinal monitoring of the granzyme B activity in luciferase-expressing tumor models receiving immune checkpoint inhibitors. We found that the bioluminescence signals generated by GBLI-2 differentiated the treatment outcome between the treated responders and non-responders. The granzyme B activity in a tumor rechallenge model was successfully imaged by GBLI-2 BLI too. GBLI-2 BLI represents a non-invasive imaging tool in animal models to facilitate immunotherapy research in addressing the challenges, such as improving response rates and preventing immune-related adverse events.

STAR★METHODS

Detailed methods are provided in the online version of this paper and include the following:

- KEY RESOURCES TABLE
- RESOURCE AVAILABILITY
  - Lead contact
  - Materials availability
  - Data and code availability
- EXPERIMENTAL MODEL AND SUBJECT DETAILS
  - Cell line
- METHOD DETAILS
  - Materials characterization
  - Synthesis of GBLI-1 and GBLI-2 probes
  - *In vitro* assay of GBLI-1 and GBLI-2 probes
  - Enzyme kinetic assay
  - Bioluminescence imaging in buffer and CT26-Luc cell lysates
  - Bioluminescence imaging in $CD8^+$ T cells
  - Western blotting
  - *In vivo* bioluminescence imaging
  - *Ex vivo* tumor analysis
  - Immunofluorescence staining of tumor tissue
- QUANTITATION AND STATISTICAL ANALYSIS

SUPPLEMENTAL INFORMATION

Supplemental information can be found online at https://doi.org/10.1016/j.chembiol.2022.08.006.

ACKNOWLEDGMENTS

This work was supported by NIH grants U54CA199075 (J.R.), R01CA243033 (J.R.), and R01CA219994 (J.I.). M.C. acknowledges the support from the Stanford Cancer Translational Nanotechnology Training Program funded by NCI award T32CA196585. L.C. was supported by a CDMRP Breast Cancer Research Program Breakthrough postdoctoral fellowship award (award no. W81XWH1810591). S.T. acknowledges the support from the Life Sciences Research Foundation. T.D. gives thanks for financial support from the Center for Molecular Analysis and Design (CMAD) at Stanford. The authors thank Stanford Shared FACS Facility for instrumentation and assistance with flow cytometry, Stanford University Mass Spectrometry for support on mass spectrometry analysis, Functional Genomics Facility at Stanford for access to LI-COR Odyssey for western blots, and Stanford Center for Innovation in In Vivo Imaging (SCI^3) for instrumentation and assistance with the Lago-X imaging system.

AUTHOR CONTRIBUTIONS

Conceptualization, M.C., K.Z., and J.R.; investigation, M.C., K.Z., S.-Y.D., S.T., P.B.B., J.X., and T.D.; writing, M.C., K.Z., S.-Y.D., P.B.B., S.T., J.I., and J.R.; methodology, F.E.I.R. and L.C.; supervision, J.I. and J.R.; funding acquisition, J.R. and J.I.

DECLARATION OF INTERESTS

The authors declare no competing interests.

Received: July 23, 2021
Revised: March 31, 2022
Accepted: August 22, 2022
Published: September 13, 2022

REFERENCES

Bagchi, S., Yuan, R., and Engleman, E.G. (2021). Immune checkpoint inhibitors for the treatment of cancer: clinical impact and mechanisms of response and resistance. Annu. Rev. Pathol. *16*, 223–249. https://doi.org/10.1146/annurev-pathol-042020-042741.

Baklaushev, V.P., Kilpeläinen, A., Petkov, S., Abakumov, M.A., Grinenko, N.F., Yusubalieva, G.M., Latanova, A.A., Gubskiy, I.L., Zabozlaev, F.G., Starodubova, E.S., et al. (2017). Luciferase expression allows bioluminescence imaging but imposes limitations on the orthotopic mouse (4T1) model of breast cancer. Sci. Rep. *7*, 7715. https://doi.org/10.1038/s41598-017-07851-z.

Bird, C.H., Rizzitelli, A., Harper, I., Prescott, M., and Bird, P.I. (2010). Use of granzyme B-based fluorescent protein reporters to monitor granzyme distribution and granule integrity in live cells. Biol. Chem. *391*, 999–1004. https://doi.org/10.1515/BC.2010.099.

Boivin, W.A., Cooper, D.M., Hiebert, P.R., and Granville, D.J. (2009). Intracellular versus extracellular granzyme B in immunity and disease: challenging the dogma. Lab Investig. *89*, 1195–1220. https://doi.org/10.1038/labinvest.2009.91.

Casciola-Rosen, L., Garcia-Calvo, M., Bull, H.G., Becker, J.W., Hines, T., Thornberry, N.A., and Rosen, A. (2007). Mouse and human granzyme B have distinct tetrapeptide specificities and abilities to recruit the bid pathway. J. Biol. Chem. *282*, 4545–4552. https://doi.org/10.1074/jbc.M606564200.

Choi, P.J., and Mitchison, T.J. (2013). Imaging burst kinetics and spatial coordination during serial killing by single natural killer cells. Proc. Natl. Acad. Sci. USA *110*, 6488–6493. https://doi.org/10.1073/pnas.1221312110.

Cullen, S.P., Brunet, M., and Martin, S.J. (2010). Granzymes in cancer and immunity. Cell Death Differ. *17*, 616–623. https://doi.org/10.1038/cdd.2009.206.

de Miguel, M., and Calvo, E. (2020). Clinical challenges of immune checkpoint inhibitors. Cancer Cell *38*, 326–333. https://doi.org/10.1016/j.ccell.2020.07.004.

Del Paggio, J.C. (2018). Immunotherapy: cancer immunotherapy and the value of cure. Nat. Rev. Clin. Oncol. *15*, 268–270. https://doi.org/10.1038/nrclinonc.2018.27.

Dragulescu-Andrasi, A., Liang, G., and Rao, J. (2009). In vivo bioluminescence imaging of furin activity in breast cancer cells using bioluminogenic substrates. Bioconjugate Chem. *20*, 1660–1666. https://doi.org/10.1021/bc9002508.

Golstein, P., and Griffiths, G.M. (2018). An early history of T cell-mediated cytotoxicity. Nat. Rev. Immunol. *18*, 527–535. https://doi.org/10.1038/s41577-018-0009-3.

He, S., Li, J., Lyu, Y., Huang, J., and Pu, K. (2020). Near-infrared fluorescent macromolecular reporters for real-time imaging and urinalysis of cancer immunotherapy. J. Am. Chem. Soc. *142*, 7075–7082. https://doi.org/10.1021/jacs.0c00659.

Hegde, P.S., Karanikas, V., and Evers, S. (2016). The where, the when, and the how of immune monitoring for cancer immunotherapies in the era of checkpoint inhibition. Clin. Cancer Res. *22*, 1865–1874. https://doi.org/10.1158/1078-0432.Ccr-15-1507.

Janiszewski, T., Kolt, S., Kaiserman, D., Snipas, S.J., Li, S., Kulbacka, J., Saczko, J., Bovenschen, N., Salvesen, G., Drag, M., et al. (2020). Noninvasive optical detection of granzyme B from natural killer cells with enzyme-activated fluorogenic probes. J. Biol. Chem. *295*, 9567–9582. https://doi.org/10.1074/jbc.RA120.013204.

Larimer, B.M., Wehrenberg-Klee, E., Dubois, F., Mehta, A., Kalomeris, T., Flaherty, K., Boland, G., and Mahmood, U. (2017). Granzyme B PET imaging as a predictive biomarker of immunotherapy response. Cancer Res. *77*, 2318–2327. https://doi.org/10.1158/0008-5472.CAN-16-3346.

Liu, H.W., Chen, L., Xu, C., Li, Z., Zhang, H., Zhang, X.B., and Tan, W. (2018). Recent progresses in small-molecule enzymatic fluorescent probes for cancer imaging. Chem. Soc. Rev. *47*, 7140–7180. https://doi.org/10.1039/c7cs00862g.

Love, A.C., and Prescher, J.A. (2020). Seeing (and using) the light: recent developments in bioluminescence technology. Cell Chem. Biol. *27*, 904–920. https://doi.org/10.1016/j.chembiol.2020.07.022.

Mac, Q.D., Mathews, D.V., Kahla, J.A., Stoffers, C.M., Delmas, O.M., Holt, B.A., Adams, A.B., and Kwong, G.A. (2019). Non-invasive early detection of acute transplant rejection via nanosensors of granzyme B activity. Nat. Biomed. Eng. *3*, 281–291. https://doi.org/10.1038/s41551-019-0358-7.

Miska, W., and Geiger, R. (1987). Synthesis and characterization of luciferin derivatives for use in bioluminescence enhanced enzyme immunoassays. New ultrasensitive detection systems for enzyme immunoassays, I. J. Clin. Chem. Clin. Biochem. *25*, 23–30. https://doi.org/10.1515/cclm.1987.25.1.23.

Ng, T.S.C., Allen, H.H., Rashidian, M., and Miller, M.A. (2022). Probing immune infiltration dynamics in cancer by in vivo imaging. Curr. Opin. Chem. Biol. *67*, 102117. https://doi.org/10.1016/j.cbpa.2022.102117.

Nguyen, A., Ramesh, A., Kumar, S., Nandi, D., Brouillard, A., Wells, A., Pobezinsky, L., Osborne, B., and Kulkarni, A.A. (2020). Granzyme B nanoreporter for early monitoring of tumor response to immunotherapy. Sci. Adv. *6*, eabc2777. https://doi.org/10.1126/sciadv.abc2777.

Nishino, M., Ramaiya, N.H., Hatabu, H., and Hodi, F.S. (2017). Monitoring immune-checkpoint blockade: response evaluation and biomarker development. Nat. Rev. Clin. Oncol. *14*, 655–668. https://doi.org/10.1038/nrclinonc.2017.88.

O'Brien, M.A., Daily, W.J., Hesselberth, P.E., Moravec, R.A., Scurria, M.A., Klaubert, D.H., Bulleit, R.F., and Wood, K.V. (2005). Homogeneous, bioluminescent protease assays: caspase-3 as a model. SLAS Discovery *10*, 137–148. https://doi.org/10.1177/1087057104271865.

Packard, B.Z., Telford, W.G., Komoriya, A., and Henkart, P.A. (2007). Granzyme B activity in target cells detects attack by cytotoxic lymphocytes. J. Immunol. *179*, 3812–3820. https://doi.org/10.4049/jimmunol.179.6.3812.

Park, H.J., Kim, K.W., Pyo, J., Suh, C.H., Yoon, S., Hatabu, H., and Nishino, M. (2020). Incidence of pseudoprogression during immune checkpoint inhibitor therapy for solid tumors: a systematic review and meta-analysis. Radiology *297*, 87–96. https://doi.org/10.1148/radiol.2020200443.

Patel, M.R., Chang, Y.F., Chen, I.Y., Bachmann, M.H., Yan, X., Contag, C.H., and Gambhir, S.S. (2010). Longitudinal, noninvasive imaging of T-cell effector function and proliferation in living subjects. Cancer Res. *70*, 10141–10149. https://doi.org/10.1158/0008-5472.CAN-10-1843.

Philip, M., and Schietinger, A. (2022). CD8+ T cell differentiation and dysfunction in cancer. Nat. Rev. Immunol. *22*, 209–223. https://doi.org/10.1038/s41577-021-00574-3.

Reddy, G.R., Thompson, W.C., and Miller, S.C. (2010). Robust light emission from cyclic alkylaminoluciferin substrates for firefly luciferase. J. Am. Chem. Soc. *132*, 13586–13587. https://doi.org/10.1021/ja104525m.

Rousalova, I., and Krepela, E. (2010). Granzyme B-induced apoptosis in cancer cells and its regulation (Review). Int. J. Oncol. *37*, 1361–1378. https://doi.org/10.3892/ijo_00000788.

Russo, V., Klein, T., Lim, D.J., Solis, N., Machado, Y., Hiroyasu, S., Nabai, L., Shen, Y., Zeglinski, M.R., Zhao, H., et al. (2018). Granzyme B is elevated in autoimmune blistering diseases and cleaves key anchoring proteins of the dermal-epidermal junction. Sci. Rep. *8*, 9690. https://doi.org/10.1038/s41598-018-28070-0.

Saida, Y., Brender, J.R., Yamamoto, K., Mitchell, J.B., Krishna, M.C., and Kishimoto, S. (2021). Multimodal molecular imaging detects early responses to immune checkpoint blockade. Cancer Res. *81*, 3693–3705. https://doi.org/10.1158/0008-5472.CAN-20-3182.

Scott, J.I., Gutkin, S., Green, O., Thompson, E.J., Kitamura, T., Shabat, D., and Vendrell, M. (2021). A functional chemiluminescent probe for in vivo imaging of natural killer cell activity against tumours. Angew. Chem. Int. Ed. *60*, 5699–5703. https://doi.org/10.1002/anie.202011429.

Sagiv-Barfi, I., Kohrt, H.E., Czerwinski, D.K., Ng, P.P., Chang, B.Y., and Levy, R. (2015). Therapeutic antitumor immunity by checkpoint blockade is enhanced by ibrutinib, an inhibitor of both BTK and ITK. Proc. Natl. Acad. Sci. USA *3*, E966–E972. https://doi.org/10.1073/pnas.1500712112.

Su, T.A., Bruemmer, K.J., and Chang, C.J. (2019). Caged luciferins for bioluminescent activity-based sensing. Curr. Opin. Biotechnol. *60*, 198–204. https://doi.org/10.1016/j.copbio.2019.05.002.

Syed, A.J., and Anderson, J.C. (2021). Applications of bioluminescence in biotechnology and beyond. Chem. Soc. Rev. *50*, 5668–5705. https://doi.org/10.1039/d0cs01492c.

Thomas, H.E., Trapani, J.A., and Kay, T.W. (2010). The role of perforin and granzymes in diabetes. Cell Death Differ. *17*, 577–585. https://doi.org/10.1038/cdd.2009.165.

Topalian, S.L., Taube, J.M., Anders, R.A., and Pardoll, D.M. (2016). Mechanism-driven biomarkers to guide immune checkpoint blockade in cancer therapy. Nat. Rev. Cancer *16*, 275–287. https://doi.org/10.1038/nrc.2016.36.

Trapani, J.A. (2001). Granzymes: a family of lymphocyte granule serine proteases. Genome Biol. *2*. https://doi.org/10.1186/gb-2001-2-12-reviews3014.

Turner, C.T., Lim, D., and Granville, D.J. (2019). Granzyme B in skin inflammation and disease. Matrix Biol. *75–76*, 126–140. https://doi.org/10.1016/j.matbio.2017.12.005.

Twomey, J.D., and Zhang, B. (2021). Cancer immunotherapy update: FDA-approved checkpoint inhibitors and companion diagnostics. AAPS J. *23*, 39. https://doi.org/10.1208/s12248-021-00574-0.

Weigelin, B., den Boer, A.T., Wagena, E., Broen, K., Dolstra, H., de Boer, R.J., Figdor, C.G., Textor, J., and Friedl, P. (2021). Cytotoxic T cells are able to

efficiently eliminate cancer cells by additive cytotoxicity. Nat. Commun. *12*, 5217. https://doi.org/10.1038/s41467-021-25282-3.

Xie, J., El Rami, F., Zhou, K., Simonetta, F., Chen, Z., Zheng, X., Chen, M., Balakrishnan, P.B., Dai, S.-Y., Murty, S., et al. (2022). Multiparameter longitudinal imaging of immune cell activity in chimeric antigen receptor T cell and checkpoint blockade therapies. ACS Cent. Sci. *8*, 590–602. https://doi.org/10.1021/acscentsci.2c00142.

Yao, H., So, M.K., and Rao, J. (2007). A bioluminogenic substrate for in vivo imaging of beta-lactamase activity. Angew. Chem. Int. Ed. *46*, 7031–7034. https://doi.org/10.1002/anie.200701931.

Yeh, H.W., and Ai, H.W. (2019). Development and applications of bioluminescent and chemiluminescent reporters and biosensors. Annu. Rev. Anal. Chem. *12*, 129–150. https://doi.org/10.1146/annurev-anchem-061318-115027.

Zambito, G., Chawda, C., and Mezzanotte, L. (2021). Emerging tools for bioluminescence imaging. Curr. Opin. Chem. Biol. *63*, 86–94. https://doi.org/10.1016/j.cbpa.2021.02.005.

Zhang, Y., He, S., Chen, W., Liu, Y., Zhang, X., Miao, Q., and Pu, K. (2021). Activatable polymeric nanoprobe for near-infrared fluorescence and photoacoustic imaging of T lymphocytes. Angew. Chem. Int. Ed. *60*, 5921–5927. https://doi.org/10.1002/anie.202015116.

Zhao, N., Bardine, C., Lourenco, A.L., Wang, Y.H., Huang, Y., Cleary, S.J., Wilson, D.M., Oh, D.Y., Fong, L., Looney, M.R., et al. (2021). In vivo measurement of granzyme proteolysis from activated immune cells with PET. ACS Cent. Sci. *7*, 1638–1649. https://doi.org/10.1021/acscentsci.1c00529.

STAR★METHODS

KEY RESOURCES TABLE

REAGENT or RESOURCE	SOURCE	IDENTIFIER
Antibodies		
Anti-mouse CD16/32	Biolegend	Cat # 101301; Clone# 93; RRID: AB_312800
Anti-CD8-FITC	Biolegend	Cat # 100705; Clone# 53–6.7; RRID: AB_312744
PE/Cyanine7 anti-mouse CD3 Antibody	Biolegend	Cat# 100219; Clone# 17A2; RRID: AB_1732068
InVivoMAb anti-mouse PD-1 (CD279)	Bio X cell	Cat# BE0146; Clone# RMP1-14; RRID: N/A
InVivoMAb anti-mouse CTLA-4 (CD152)	Bio X cell	Cat# BE0164; Clone# 9D9; RRID: N/A
Rat anti-mouse CD8-alpha	Bio-Rad	Cat# MCA609GT; Clone# KT15; RRID: AB_321407
Anti-Granzyme B antibody	Abcam	Cat# ab4059; Clone# N/A; RRID: N/A
Goat anti-Rat IgG (H+L) Cross-Adsorbed Secondary Antibody, Cyanine5	Thermo Fisher Scientific	Cat# A10525; Clone# N/A; RRID:AB_2534034
Goat anti-Rabbit IgG (H+L) Cross-Adsorbed Secondary Antibody, Alexa Fluor™ 594	Thermo Fisher Scientific	Cat# A-11012; Clone#: N/A; RRID: AB_2534079
Donkey anti-mouse IgG IRDye 680	LI-COR	Cat# 926-68072; Clone# N/A; RRID: AB_2814912
Goat anti-rabbit IgG IRDye 800CW	LI-COR	Cat# 926-32211; Clone# N/A; RRID: AB_2651127
Chemicals, peptides, and recombinant proteins		
HEPES	Sigma-Aldrich	Cat# H4034; CAS: 7365-45-9
Triton X-100	Sigma-Aldrich	Cat# P93443; CAS:9036-19-5
TWEEN 20	Sigma-Aldrich	Cat# P9416; CAS:9005-64-5
4% Paraformaldehyde solution	Thermo Scientific	Cat# AAJ61899AK; CAS: 30525-89-4
D-luciferin potassium salt	GoldBio	Cat# LUCK®; CAS: 115144-35-9
RPMI 1640 Medium, HEPES	GIBCO	Cat# 22400089
Ac-IEPD-CHO	BioVision	Cat# 1119-1
ATP disodium salt	Sigma-Aldrich	Cat# BML-P134-0005
PMA	Sigma-Aldrich	Cat# P1585; CAS: 16561-29-8

(*Continued on next page*)

Continued

REAGENT or RESOURCE	SOURCE	IDENTIFIER
ionomycin	Sigma-Aldrich	Cat# 407952; CAS: 56092-82-1
Brefeldin A	Sigma-Aldrich	Cat# B6542; CAS: 20350-15-6
Firefly luciferase	Sigma-Aldrich	Cat# 22400105
Recombinant Mouse Caspase-1 Protein	Novus Biological	Cat# NBP1-99607
Recombinant Mouse BID (Caspase-8-cleaved) Protein	R&D systems	Cat# 883M8050
Recombinant Mouse Granzyme A (Gzma)	Cusabio	Cat# CSB-EP010081MO
Recombinant Mouse Granzyme B Protein, CF	R&D systems	Cat# 1865-SE-010
Recombinant Mouse Active Cathepsin C/DPPI Protein	R&D systems	Cat# 2336-CY-010
Dynabeads Mouse T-Activator CD3/CD28	Life Technologies	Cat# 11453D
IL-2	PeproTech	Cat# 212-12
IL-7	Pepro Tech	Cat# 217-17
Experimental models: Cell lines		
Mouse CT26-Luc cell		Cat# N/A; RRID: N/A
Mouse 4T1-Luc cell	Edward Graves et al. Cell Rep. 2014; 8(2): 402-409.	Cat# N/A; RRID: N/A
Experimental models: Organisms/strains		
BALB/c mouse	The Jackson Laboratory	IMSR_JAX:000651
NU/NU Nude mouse, Crl: NU-*Foxn1*^{nu}	Charles River	088 (Homozygous)
NSG mouse (NOD.Cg-Prkdc^{scid}Il2rg^{tm1Wjl}/SzJ)	The Jackson Laboratory	IMSR_JAX:005557
Software and algorithms		
GraphPad Prism 7 Software	GraphPad Software	http://www.graphpad.com
ImageJ	NIH	http://imagej.nih.gov/ij/index.html
FlowJo 10.5.0 software	Tree Star	https://www.flowjo.com

RESOURCE AVAILABILITY

Lead contact

All requests for reagents and resources should be directed to the lead contact, Jianghong Rao (jrao@stanford.edu).

Materials availability

GBLI-1 and GBLI-2 probes generated in this study will be available from the lead contact upon request.

Data and code availability

- All data reported in this paper will be shared by the lead contact upon request.
- This paper does not report original code.
- Any additional information required to reanalyze the data reported in this paper is available from the lead contact upon request.

EXPERIMENTAL MODEL AND SUBJECT DETAILS

Cell line

CT26-Luc cell line (female) was a kind gift from Dr. Sanjiv Sam Gambhir' Laboratory and 4T1-luc (female) was from Dr. Edward Graves' Laboratory. All cell lines were cultured in RPMI-1640 medium (Catalog # 22400089, GIBCO) with 10% FBS and 1% pen/strep. Cells were cultured at 37 °C in a sterile incubator containing 5% CO_2. Mycoplasma test was carried out routinely to detect contamination (MycoAlert Mycoplasma Detection Kit purchased from Lonza).

METHOD DETAILS

Materials characterization

High performance liquid chromatography (HPLC) analyses were performed on a Dionex Ultimate 300 HPLC System (Thermo Scientific) equipped with a GP50 gradient pump and an in-line diode array UV-Vis detector. Reverse-phase C18 (Phenomenex, 5 μm, 4.6 × 250 mm or Dionex, 5 μm, 21.2 × 250 mm) columns were used with acetonitrile/water gradient mobile phase containing 0.1% trifluoroacetic acid (at a flow rate of 1 or 10 mL/min for analysis or purification respectively). Proton nuclear magnetic resonance (^{1}H NMR) and carbon nuclear magnetic resonance (^{13}C NMR) spectra were recorded on Inova 500/600 MHz NMR spectrometers at NMR facility of Stanford University. ^{1}H NMR spectra are reported as follows: chemical shifts are reported as δ in units of parts per million (ppm). Multiplicities are reported as follows: s (singlet), d (doublet), t (triplet), q (quartet), dd (doublet of doublets) or m (multiplet); coupling constants are reported as a J value in Hertz. Liquid chromatography mass spectrometry (LC-MS, Waters Corporation) and high-resolution mass spectrometry (HRMS, Waters Corporation) analyses were performed at the Mass Spectrometry Facility of Stanford University. Fluorescence images of tissue section were obtained on Laser Scanning Microscope LSM710 (Zeiss). Flow cytometry assays were acquired on FACS Calibur flow cytometry (Becton Dickinson, USA). *In vivo* animal bioluminescence images were captured using a Lago-X system (Spectral, Tucson, AZ).

Synthesis of GBLI-1 and GBLI-2 probes

The synthetic routes for GBLI-1 and GBLI-2 are shown in Scheme S1.

Synthesis of (4*S*,7*S*,10*S*,13*S*)-10-benzyl-7-(3-(*tert*-butoxy)-3-oxopropyl)-4-((*S*)-sec-butyl)-13- ((2-cyanobenzo[d]thiazol-6-yl)carbamoyl)-2,5,8,11-tetraoxo-3,6,9,12-tetraazapentadecan-15-oate (1)To a 50 mL two-necked round bottom flask was added Ac-IEFD-OH (0.2 mmol, 135.4 mg) and 4-methylmorpholine (0.4 mmol, 40.5 mg). The flask was placed under nitrogen (3 × vacuum/fill cycles) and was cooled to 0°C. Isobutyl chloroformate (0.2 mmol, 27.3 mg) was added in portions at 0°C, causing the white suspension to turn light yellow. The yellow suspension was stirred at 0°C for 30 min and then 6-amino-2-cyanobenzothiazole (0.3 mmol, 52.6 mg) was added in portions over 1 h at 0°C, and the reaction mixture was warmed to r.t. naturally, stirred overnight. The final product **1** was purified by preparative-HPLC to afford a white powder (21.8 mg, 13%). ^{1}H NMR (600 MHz, DMSO-d_6) δ 10.39 (s, 1H), 8.73 (d, *J* = 2.0 Hz, 1H), 8.42 (d, *J* = 7.8 Hz, 1H), 8.17 (d, *J* = 9.0 Hz, 1H), 7.96 (d, *J* = 7.7 Hz, 1H), 7.89 (dd, *J* = 8.1, 3.7 Hz, 2H), 7.76 (dd, *J* = 9.1, 2.1 Hz, 1H), 7.18–7.15 (m, 2H), 7.12 (dd, *J* = 8.4, 6.7 Hz, 2H), 7.09–7.05 (m, 1H), 4.71 (q, *J* = 7.4 Hz, 1H), 4.48 (ddd, *J* = 9.2, 7.8, 4.7 Hz, 1H), 4.16 (td, *J* = 8.1, 5.4 Hz, 1H), 4.08 (t, *J* = 7.8 Hz, 1H), 2.98 (dd, *J* = 14.0, 4.6 Hz, 1H), 2.81–2.73 (m, 2H), 2.52 (dd, *J* = 16.0, 7.5 Hz, 1H), 2.09 (dt, *J* = 9.7, 6.1 Hz, 2H), 1.82 (s, 3H), 1.75 (ddt, *J* = 15.4, 10.0, 6.1 Hz, 1H), 1.62 (ddt, *J* = 14.0, 10.0, 7.7 Hz, 2H), 1.38–1.34 (m, 1H), 1.32 (s, 9H), 1.32 (s, 9H), 1.03 (ddt, *J* = 16.2, 14.4, 7.5 Hz, 1H), 0.78–0.70 (m, 6H). MS: *m/z* calc'd for $C_{42}H_{56}N_7O_9S$ [M + H]$^+$, 834.4; found 834.4.

Synthesis of (S)-2-(6-((2,5,8,11S)-5-benzyl-11-((S)-sec-butyl)-8-(2-carboxyethyl)-2-(carboxymethyl)-4,7,10,13-tetraoxo-3,6,9,12-tetraazatetradecanamido)benzo[d]thiazol-2-yl)-4,5-dihydrothiazole-4-carboxylic acid (GBLI-1)

Compound **1** was added to a solution of CF_3COOH: CH_2Cl_2: TIPS = 1: 1: 0.05 and stirred at r.t. for 2 h. After concentration *in vacuo*, the residue was precipitated in ether and used in the next step without further purification.

To a solution of the residue and D-Cys-OH (0.05 mmol, 12.2 mg) in DMF/H_2O (v/v = 1/1, 5 mL) was added saturated $NaHCO_3$ aqueous solution to adjust pH to 7-8, The reaction mixture was stirred at r.t. for 2 h, and the final product GBLI-1 was purified by preparative-HPLC to afford a light-yellow powder (13.5 mg, 62%). ^{1}H NMR (500 MHz, DMSO-d_6) δ 10.31 (s, 1H), 8.64 (d, *J* = 2.0 Hz, 1H), 8.50 (d, *J* = 7.3 Hz, 1H), 8.10 (d, *J* = 8.9 Hz, 1H), 8.04 (d, *J* = 7.7 Hz, 1H), 7.94 (dd, *J* = 8.1, 4.0 Hz, 2H), 7.68 (dd, *J* = 9.0, 2.1 Hz, 1H), 7.22 (d, *J* = 7.2 Hz, 2H), 7.17 (t, *J* = 7.4 Hz, 2H), 7.12 (t, *J* = 7.1 Hz, 1H), 5.43 (dd, *J* = 9.7, 8.3 Hz, 1H), 4.70 (q, *J* = 7.2 Hz, 1H), 4.50 (td, *J* = 8.2, 4.7 Hz, 1H), 4.20 (td, *J* = 8.1, 5.5 Hz, 1H), 4.11 (t, *J* = 7.9 Hz, 1H), 3.78 (dd, *J* = 11.3, 9.8 Hz, 1H), 3.69 (dd, *J* = 11.2, 8.2 Hz, 1H), 3.03 (dd, *J* = 14.1, 4.5 Hz, 1H), 2.85–2.76 (m, 2H), 2.60 (dd, *J* = 16.6, 7.6 Hz, 1H), 2.21–2.07 (m, 2H), 1.85 (s, 4H), 1.68 (dt, *J* = 18.6, 7.0 Hz, 2H), 1.38 (ddd, *J* = 13.5, 7.5, 3.7 Hz, 1H), 1.05 (dt, *J* = 13.4, 7.7 Hz, 1H), 0.79–0.70 (m, 6H). ^{13}C NMR (125 MHz, DMSO-d_6) δ 174.50, 171.97, 171.82, 171.60, 171.47, 170.10, 170.00, 164.92, 159.63, 149.16, 138.67, 137.87, 136.71, 129.61, 128.46, 126.72, 124.65, 120.32, 112.11, 78.56, 57.50, 54.33, 52.42, 51.20, 37.83, 36.68, 36.35, 35.22, 30.48, 27.57, 24.92, 22.94, 15.82, 11.43. HRMS: *m/z* calc'd for $C_{37}H_{42}N_7O_{11}S$ [M + H]$^-$,824.2462; found 824.2386.

Synthesis of *Tert*-butyl (4,*7,10*,13*S*)-10-benzyl-7-(3-(*tert*-butoxy)-3-oxopropyl)-4-((*S*)-*sec*-butyl)-13-((4-(hydroxymethyl)phenyl) carbamoyl)-2,5,8,11-tetraoxo-3,6,9,12-tetraazapentadecan-15-oate (2)

To a solution of peptide Ac-IEFD-OH (0.2 mmol, 135.4 mg) and 4-aminobenzyl alcohol (PABA) (0.6 mmol, 73.9 mg) in CH_2Cl_2 was added 2-ethoxy-1-ethoxycarbonyl-1,2-dihydroquinoline (EEDQ) (0.6 mmol, 148.4 mg), and was rigorously stirred at r.t. for 5 h. The final product **1** was purified by flash column chromatography (Hexane/ethyl acetate = 1: 1, MeOH/CH_2Cl_2 = 20: 1, v/v) to yield compound **1** as a white solid (150.3 mg, 96%). ^{1}H NMR (500 MHz, DMSO-d_6) δ 9.88 (s, 1H), 8.40 (d, *J* = 8.0 Hz, 1H), 8.04 (d, *J* = 7.6 Hz, 1H), 7.95 (dd, *J* = 22.2, 8.0 Hz, 2H), 7.58 (d, *J* = 8.3 Hz, 2H), 7.25 (d, *J* = 8.3 Hz, 2H), 7.18 (ddd, *J* = 23.0, 15.2, 7.0 Hz, 5H), 4.71 (q, *J* = 7.4 Hz, 1H), 4.52 (td, *J* = 8.4, 4.5 Hz, 1H), 4.44 (s, 2H), 4.21 (q, *J* = 7.3 Hz, 1H), 4.13 (t, *J* = 7.7 Hz, 1H), 3.01 (dd, *J* = 13.9, 4.5 Hz, 1H), 2.82 (dd, *J* = 14.0, 9.2 Hz, 1H), 2.74 (dd, *J* = 15.8, 6.9 Hz, 1H), 2.58–2.52 (m, 1H), 2.14 (dt, *J* = 9.9, 4.9 Hz, 2H), 1.87 (s, 3H), 1.85–1.75 (m, 1H), 1.67 (q, *J* = 6.3, 4.9 Hz, 2H), 1.44–1.40 (m, 1H), 1.39 (s, 9H), 1.36 (s, 9H), 1.08 (dt, *J* = 14.5, 7.7 Hz, 1H), 0.82–0.75 (m, 6H). MS: *m/z* calc'd for $C_{41}H_{60}N_5O_{10}$ [M + H]$^+$, 782.4; found 782.6.

Synthesis of Tert-*butyl (4,7,10,13*S*)-10-benzyl-7-(3-(*tert-*butoxy)-3-oxopropyl)-4-((*S*)-*sec-*butyl)-13-((4-(((2-cyanobenzo[d]thiazol-6-yl)oxy)methyl)phenyl)carbamoyl)-2,5,8,11-tetraoxo-3,6,9,12-tetraazapentadecan-15-oate (3)*

To a stirring solution of compound **2** (66 mg, 0.08 mmol) in extra dry CH_2Cl_2 (20 mL) at 0°C under argon protection was added triethylamine (Et_3N) (55 μL, 0.4 mmol), followed by the slow dropwise addition of methanesulfonyl chloride (30 μL, 0.4 mmol). The reaction mixture was stirred at 0°C for an additional 2 h and then allowed to warm to r.t. for 18 h. The solvent was removed *in vacuo* and the residue was dissolved in a large amount of ethyl acetate. Then the solution was washed successively with 50 mL 5% aqueous citric acid solution and 50 mL 5% aqueous $NaHCO_3$ solution. The organic layer was dried over $MgSO_4$ and concentrated *in vacuo*. The crude product was used in the next step without further purification.

To a solution of obtained residue in extra dry DMF (5 mL) was added 2-cyano-6-hydroxybenzothiazole (18 mg, 0.1 mmol), K_2CO_3 (30 mg, 0.2 mmol) and KI (1 mg, 0.06 mmol). Then the reaction mixture was stirred at room temperature for 18 h. After concentrated *in vacuo*, the residue was dissolved in ethyl acetate and washed with water, then concentrated *in vacuo*. The residue was purified by flash column chromatography (Hexane/ethyl acetate = 1: 1, MeOH/CH_2Cl_2 = 20: 1, v/v) to yield compound **3** as a pale-yellow solid (39 mg, 52%). ^{1}H NMR (500 MHz, DMSO-d_6) δ 10.00 (s, 1H), 8.41 (d, J = 7.9 Hz, 1H), 8.16 (d, J = 9.1 Hz, 1H), 8.04 (d, J = 7.6 Hz, 1H), 8.01–7.96 (m, 2H), 7.93 (d, J = 7.8 Hz, 1H), 7.67 (d, J = 8.3 Hz, 2H), 7.45 (d, J = 8.5 Hz, 2H), 7.39 (dd, J = 9.1, 2.5 Hz, 1H), 7.21 (d, J = 7.1 Hz, 2H), 7.17 (t, J = 7.4 Hz, 2H), 7.11 (t, J = 7.0 Hz, 1H), 5.18 (s, 2H), 4.71 (q, J = 7.5 Hz, 1H), 4.55–4.48 (m, 1H), 4.21 (q, J = 7.3 Hz, 1H), 4.12 (t, J = 7.7 Hz, 1H), 3.01 (dd, J = 13.9, 4.5 Hz, 1H), 2.85–2.73 (m, 2H), 2.58–2.52 (m, 1H), 2.14 (dt, J = 10.2, 5.5 Hz, 2H), 2.00 (s, 1H), 1.87 (s, 3H), 1.80 (s, 1H), 1.68 (dd, J = 15.9, 8.3 Hz, 2H), 1.38 (s, 9H), 1.36 (s, 9H), 1.06 (dq, J = 15.7, 7.6 Hz, 1H), 0.81–0.76 (m, 6H). MS: *m/z* calc'd for $C_{49}H_{60}N_7O_{10}S$ [M + H]$^-$, 938.4; found 938.6.

*Synthesis of (*S*)-2-(6-((4-((2*S*,5*S*,8*S*,11*S*)-5-benzyl-11-((*S*)-*sec-*butyl)-8-(2-carboxyethyl)-2-(carboxymethyl)-4,7,10,13-tetraoxo-3,6,9,12-tetraazatetradecanamido)benzyl)oxy) benzo[d]thiazol-2-yl)-4,5-dihydrothiazole-4-carboxylic acid (GBLI-2)*

The similar reaction described above to prepare compound GBLI-1 was used, and final compound GBLI-2 was purified by preparative-HPLC to afford a yellow powder (20 mg, 55%). ^{1}H NMR (500 MHz, DMSO-d_6) δ 9.95 (s, 1H), 8.45 (d, J = 7.5 Hz, 1H), 8.06 (dd, J = 8.4, 6.6 Hz, 2H), 7.94 (dd, J = 15.7, 7.9 Hz, 2H), 7.86 (d, J = 2.6 Hz, 1H), 7.67 (dd, J = 8.0, 5.9 Hz, 2H), 7.49–7.42 (m, 2H), 7.29–7.10 (m, 6H), 5.43 (dd, J = 9.8, 8.3 Hz, 1H), 5.16 (s, 2H), 4.67 (q, J = 7.1 Hz, 1H), 4.52–4.46 (m, 1H), 4.21 (q, J = 7.4, 6.9 Hz, 1H), 4.12 (t, J = 7.9 Hz, 1H), 3.78 (dd, J = 11.3, 9.8 Hz, 1H), 3.69 (dd, J = 11.2, 8.3 Hz, 1H), 3.03 (dd, J = 14.0, 4.6 Hz, 1H), 2.80 (td, J = 16.1, 15.5, 7.7 Hz, 2H), 2.58 (dd, J = 16.5, 7.5 Hz, 1H), 2.18 (dq, J = 16.5, 10.6 Hz, 2H), 1.86 (s, 4H), 1.74–1.63 (m, 2H), 1.39 (ddd, J = 12.3, 7.5, 3.7 Hz, 1H), 1.06 (dq, J = 15.2, 7.7 Hz, 1H), 0.81–0.73 (m, 6H). ^{13}C NMR (125 MHz, DMSO-d_6) δ 174.51, 172.02, 171.87, 171.66, 171.61, 171.37, 170.05, 169.61, 164.89, 158.43, 158.38, 147.63, 139.18, 137.86, 137.56, 131.78, 129.62, 129.08, 128.46, 126.71, 125.26, 119.81, 118.02, 106.33, 78.54, 70.22, 57.54, 54.38, 52.48, 51.08, 37.79, 36.67, 36.40, 35.19, 30.50, 27.53, 24.93, 22.94, 15.83, 11.43. HRMS: *m/z* calc'd for $C_{44}H_{48}N_7O_{12}S_2$ [M + H]$^-$, 930.2881; found 930.2807.

In vitro assay of GBLI-1 and GBLI-2 probes

Pro-granzyme B (R&D systems, 1865-SE) was activated to granzyme B using cathepsin C (R&D systems) following the manufacturer's protocol. GBLI-1 or GBLI-2 probes were incubated with the active granzyme B enzyme (22 nM) in 50 mM Tris buffer (pH 7.4) over 0.5, 3, 6, 12, and 24 h. The cleaved reactions were analyzed by HPLC.

To evaluate the specificity of the probes for granzyme B, GBLI-1 and GBLI-2 probes (10 μM) were incubated with 0.8 μg/mL of various enzymes: the activated forms of granzyme A (Cusabio) and granzyme B (R&D system) in 50 mM Tris buffer (pH 7.4); caspase-1 (Novus Biological), caspse-3 (Sigma), and caspase 8 (R&D systems) in 50 mM HEPES buffer (pH 7.4) with 0.5% CHAPS, 1 mM EDTA, 100 mM NaCl, 10% glycerol, and 10 mM DTT; and cathepsin C (R&D systems) in 50 mM MES buffer (pH 5.5) with 50 mM NaCl. After 24 h incubation at 37°C, luciferase buffer was added to give a final concentration of 100 nM luciferase, 1 mM ATP, and 10 mM $MgCl_2$. Immediately after mixing, the bioluminescence signals were detected using a microplate reader (SpectraMax®iD5 microplate reader, Molecular Devices, USA).

To block granzyme B activity, its inhibitor Ac-IEPD-CHO (1119-1, BioVision) at 100 μM was pretreated with granzyme B (22 nM), then the mixture was incubated with GBLI-1 or GBLI-2 probes (10 μM). After 24 h incubation at 37°C, luciferase buffer was added to give a final concentration of 100 nM luciferase, 1 mM ATP, and 10 mM $MgCl_2$. Immediately after mixing, the bioluminescence signals were detected using a microplate reader (SpectraMaxiD5 microplate reader, Molecular Devices, USA).

Enzyme kinetic assay

Various concentrations of GBLI-1 and GBLI-2 probes (2, 5, 10, 20, 40, 60, 80, 100,120, μM) in Tris buffer (50 mM, pH 7.4) were incubated with granzyme B (50 nM) at a final volume of 30 μL. The fluorescence of the cleaved products, amino-luc (Ex: 360, Em: 520) or D-luc (Ex: 320, Em: 530), were monitored in real time at 37°C for 30 min using a microplate reader (SpectraMax®iD5 microplate reader, Molecular Devices, USA). The linear region of the curve was used to calculate the reaction rate using Michaelis-Menten equation in GraphPad Prism. All measurements were repeated three times and the data are presented as the mean with standard deviation (SD).

Bioluminescence imaging in buffer and CT26-Luc cell lysates

To image granzyme B in buffer, GBLI-1 and GBLI-2 probes were preincubated with mouse granzyme B (22 nM) in Tris buffer (50 mM, pH 7.4) overnight. Then the mixture buffer was added with 100 μg/mL luciferase, 1 mM ATP, and 10 mM $MgCl_2$ for dynamic bioluminescence imaging over 90 min.

To image granzyme B in CT26-Luc cell lysates, GBLI-1 and GBLI-2 probes (10 μM) were preincubated with mouse granzyme B (22 nM) in Tris buffer (50 mM, pH 7.4) overnight. CT26-Luc cells were harvested by centrifugation and the pellets were washed in cold-phosphate-buffered saline (PBS) twice. The pellets were resuspended in 150 μL of NP-40 lysis buffer (50 mM Tris buffer containing 150 mM NaCl and 1% Triton-100, pH 7.4) for 20 min on ice. Then the lysates were centrifuged at 15,000 × g for 15 min and the supernatants were collected. The supernatants were added into the preincubation buffer containing GBLI probes and mouse granzyme B in 50 mM Tris buffer (pH 7.4) for dynamic bioluminescence imaging over 90 min.

Bioluminescence imaging in $CD8^+$ T cells

To collect $CD8^+$ T cells, spleens from transgenic BALB/c female mice (*Fluc* + lymphocytes) were gently dissociated using 70 μm cell strainers and centrifuged at 300 × g for 5 min. Single-cell suspensions were enriched for *Fluc*+ $CD8^+$ T cells using the EasySep Mouse $CD8^+$ T Cell Negative Isolation Kit (Catalog # 19,853, StemCell Technologies, USA) according to the manufacturer's protocol. Isolated *Fluc*+ $CD8^+$ T cells were either used at this preparation endpoint (Resting $CD8^+$ T cells) or activated for 48 h with Dynabeads Mouse T-Activator CD3/CD28 (Life Technologies, Grand Island, NY) in the presence of murine IL-2 (10 ng/mL) and murine IL-7 (10 ng/mL; PeproTech, USA) in RPMI 1640 media supplemented with 10% heat-inactivated FBS, 1 mmol/L sodium pyruvate, 2 mmol/L glutamine, 100 U/mL penicillin, and 100 μg/mL streptomycin. All cells were cultured in a humidified incubator at 37°C and 5% CO_2. Dyna beads were removed after two rounds of magnetic binding and cells were rested 72 h in fresh medium containing IL-2 and IL-7 before use.

To verify $CD8^+$ T cells, the single-cell suspensions were kept in phosphate-buffered saline (PBS) supplemented with 2% fetal bovine serum. Cells were blocked with Fc receptor blocking reagent (TruStain FcX™ (anti-mouse CD16/32) Antibody, Biolegend, USA) and incubated for 30 min on ice with FITC anti-CD8 (clone 53–6.7) and PE/Cy7 anti-CD3 (clone 17A2). Unstained sample of T cells was used as control. All antibodies were purchased from Biolegend. Samples were acquired on a BD LSR II flow cytometer (BD Biosciences), and analysis was performed with FlowJo 10.5.0 software (Tree Star).

To detect the granzyme B activity, isolated $CD8^+$ T cells were harvested by centrifugation and the pellets were washed in cold-phosphate-buffered saline (PBS) twice. The pellets were divided into three parts. The first part of cells was used for granzyme B detection in living cells. The living cells were incubated with GBLI-1 or GBLI-2 probes. The second part of cells was resuspended in 150 μL of NP-40 lysis buffer (50 mM Tris buffer containing 150 mM NaCl and 1% Triton-100, pH 7.4). The lysates were centrifuged at 15,000 × g for 15 min, and the supernatants were collected. To aliquots of supernatants were added GBLI-1 or GBLI-2 probes (10 μM) in 50 mM Tris buffer (pH 7.4) for granzyme B detection over 90 min. The remaining cells were used for western blotting assay.

Western blotting

CT26-Luc and $CD8^+$ T Cells were washed 3 times with ice-cold PBS and lysed in RIPA buffer. Protein concentrations of centrifuged whole lysates were determined by BCA assay. $CD8^+$ T cell lysate were loaded each lane in NuPAGE 4-12% Bis-Tris protein gels for electrophoresis at 200V for 90 min. Wet transfer was performed using a Bio-Rad transfer kit at 300 mA for 90 min. The transferred nitrocellulose membrane was blocked in PBS containing 5% BSA and 0.1% Tween 20 for 1 h. Primary antibody incubation was performed in the blocking buffer overnight at 4°C at the recommended concentration. The membrane was then washed with PBS containing 0.1% Tween 20 for 5 min, four times. Secondary antibody incubation (LI-COR donkey anti-mouse IgG IRDye 680 or anti-rabbit IgG IRDye 800CW, 1: 10,000) was performed in the blocking buffer for 2 h at room temperature. After washing four times with PBS containing 0.1% Tween 20, membranes were analyzed on an LI-COR Odyssey imaging system.

In vivo bioluminescence imaging

All mouse experimental procedures were approved by the Institutional Animal Care and Use Committee (IACUC), Stanford University. 7-8 weeks female BALB/c mice were purchased from Jackson Laboratory, USA. All bioluminescence images were captured by an SPECTRAL Lago X Imaging System (Spectral Instrumental Imaging, Tucson, AZ) at 10-15 min after the probe injection and the imaging data were analyzed by Aura Imaging Software developed by Spectral Instrumental Imaging. Tumor diameters were monitored every two days and the volume (V) was calculated using the formula $V = ½ \times \text{length} \times (\text{width})^2$.

For CT26-Luc models, one million CT26-Luc cells were subcutaneously inoculated into the right back of BABL/c mice. At day 12 after tumor inoculation, when the tumor volume reaches about 200 mm^3, mice were randomly grouped into treated and untreated groups. Each mouse in the treated group (20 mice) received intraperitoneal (i.p) injection of PD-1 (200 μg/mouse) and CLTA-4 (100 μg/mouse) checkpoint inhibitor antibodies in each treatment on day 12, 15, and 17 after tumor inoculation (three times in total). The untreated mice (5 mice in total) were i.p injected with saline at the same time points. *In vivo* bioluminescence imaging was performed on day 11, 14, 17, 20, and 23 after tumor inoculation. On each imaging day, the mice were intravenously (i.v) injected with GBLI-2 (10 mg/kg) for bioluminescence imaging of granzyme B activity. At 2 h after GBLI-2 injection, the mice were then i.p injected with D-luciferin (150 mg/kg) for bioluminescence imaging of luciferase activity. At the end of bioluminescence imaging, the treated mice were classified as non-responsive when the GBLI-2 signal was similar to that in untreated tumors, and as responsive when the GBLI-2 signal was higher than that in untreated tumors.

For rechallenge study, on day 110 after tumor inoculation, the cured mice were rechallenged with 1×10^6 CT26-Luc cells or 1×10^6 4T1-Luc cells. Bioluminescence imaging was performed on day 1, 2, 4, 6 after tumor rechallenge. On each imaging day, the mice were intravenously (i.v) injected with GBLI-2 (10 mg/kg) for bioluminescence imaging. At 2 h after GBLI-2 injection, the mice were then i.p injected with D-luciferin (150 mg/kg) for bioluminescence imaging of luciferase activity.

In vivo bioluminescent images were acquired using a Lago-X system. The imaging parameters was followed: Exposure time = 60 s, Binning = medium (8 × 8), Imaging Field of View (FOV) = 25 × 25 cm for GBLI-2 probes; Exposure time = 10 s, Binning = medium (8 × 8), FOV = 25 × 25 cm for D-luciferin probes. Imaging commenced 10-15 min post injection of GBLI-2 or D-luciferin when the light output was relatively stable. All mice were positioned on their tumor side (Right side).

Ex vivo tumor analysis

Single cell suspensions from the tumors were obtained by enzymatic digestion with 400 U/mL of type D collagenase (Roche) and 0.25 mg/mL of DNAse I (Roche) in HBBS buffer (Corning) at 37°C for 1 h. Digestion reaction was stopped by adding 5 mM of EDTA (Corning) followed by washing with RPMI 1640 medium containing 10% heat-inactivated FBS (GIBCO), 2 mM of L-glutamine (Corning), 100 IU of Penicillin (Corning) and 100 mg/mL of Streptomycin (Corning). Cellular suspension was filtered through a 70 μm filter to remove adipocytes and aggregated cellular debris. $CD45^+$ cells from each sample were quantified using Count Bright Absolute Counting beads (Thermo Fisher Scientific).

To stain intracellular cytokine, tumor cell suspensions were stimulated with 100 ng/mL of PMA (Sigma-Aldrich) and 500 ng/mL of ionomycin (Sigma-Aldrich) for 4 h in the presence of Brefeldin A (10 μg/mL) to allow the accumulation of intracellular cytokines. Following stimulation, the cells were washed and incubated with 2.4G2 mAb for 10 min at 4°C to block Fc receptors. Cells were stained with monoclonal antibodies (mAbs) against surface markers at 4°C for 20 min. After staining of surface markers, cells were fixed, permeabilized, and stained for granzyme B at 4°C for 35 min. Stained cells were acquired on a LSRFortessa X20 (BD Biosciences), and data was analyzed with FlowJo Software.

Immunofluorescence staining of tumor tissue

The harvested tumor samples were flash-frozen in Tissue-Tek O.C.T at −20°C, and frozen tissues were sectioned using a cryostat to obtain 6-μm slices. The tumor sections were fixed with cold 4% PFA and permeabilized by incubating with PBS containing 0.1% Triton X-100 for 10 min. After washing tissue three times with PBS, the samples were incubated for 1 h with 1% bovine serum albumin (BSA) and 3% goat serum in PBS containing 0.1% Tween 20 (PBST) to block nonspecific binding of antibodies. The sectioned samples were then stained with primary antibody anti-rat CD8 (Clone KT15, Bio-Rad, 1:1000 diluted in PBST) and anti-rabbit granzyme B (ab4059, Abcam, 1:500 diluted in PBST) at 4°C overnight. Following this, the samples were incubated with secondary antibody goat anti-rat Cy5 (A10525, Thermo Fisher Scientific, 1:500 diluted in PBST) and goat anti-rabbit Alexa Fluor 594 (A-11012, Thermo Fisher Scientific, 1:1000 diluted in PBST) for 1 h at room temperature. After three-time washes, cell nuclei were stained with DAPI (300 nM, 15 min). The tumor sections were then mounted with ProLong™ gold antifade mountant. Fluorescence imaging was performed on a Zeiss LMS710 confocal microscope, and images were analyzed using ImageJ software.

QUANTITATION AND STATISTICAL ANALYSIS

The data were expressed as mean ± SD Statistical calculation of experimental data was using the One-way ANOVA statistical analysis. The data were classified as p values and denoted by (*) for $p < 0.05$, (**) for $p < 0.01$ and (***) for $p < 0.001$.